M 2020

U.PORTO
FEUP FACULDADE DE ENGENHARIA
UNIVERSIDADE DO PORTO

DESIGN OF PRESSURE TEMPERATURE SWING ADSORPTION PROCESS FOR METHANE UPGRADE

MARIANA CAROLINA NUNES BESSA
DISSERTAÇÃO DE MESTRADO APRESENTADA
À FACULDADE DE ENGENHARIA DA UNIVERSIDADE DO PORTO EM
ENGENHARIA QUÍMICA

Master in Chemical Engineering

Design of Pressure Temperature Swing Adsorption process for methane upgrade

Master dissertation

of

Mariana Carolina Nunes Bessa

Developed within the course of dissertation

held in

LSRE-LCM - Laboratory of Separation and Reaction Engineering - Laboratory of Catalysis and Materials

Supervisors: **Doutor Alexandre Ferreira**

Professora Ana Mafalda Ribeiro

Professor Alírio Rodrigues

U.PORTO
FEUP FACULDADE DE ENGENHARIA
UNIVERSIDADE DO PORTO

DEPARTAMENTO DE
ENGENHARIA QUÍMICA

July 2020

Acknowledgment

First, I would like to thank my Professors Ana Mafalda Ribeiro e Alexandre Ferreira, not only for the great opportunity to work in the LSRE-LCM laboratories, but also for the guidance, the contribution of knowledge and their availability during the making of this thesis.

To Idelfonso Nogueira, for the warm welcome at the laboratories and all the help given, whenever I needed.

To my parents and siblings, Beatriz e Manel, for being fundamental pillars in my life, especially throughout this five-year journey.

To my boyfriend, Bruno, for all the support and optimism that were essential in this journey.

To Rita, Joana, Ramos, Cerqueira, Bruno and Martins for all the companionship, comprehension and motivation.

This work was financially supported: by Project NORTE-01-0145-FEDER-029384 funded by FEDER funds through NORTE 2020 - Programa Operacional Regional do NORTE – and by national funds (PIDDAC) through FCT/MCTES and by Base Funding - UIDB/50020/2020 of the Associate Laboratory LSRE-LCM - funded by national funds through FCT/MCTES (PIDDAC).

Abstract

The liquefaction and transport of natural gas require a pre-treatment to remove impurities, such as nitrogen and carbon dioxide, that could damage pipelines and equipment. Multicolumn cryogenic distillation processes are used for the production of methane streams with less than 50 ppm of carbon dioxide, which is one of the requirements for the liquified natural gas (LNG) transport. Cyclic adsorption-based processes, namely pressure temperature swing adsorption (PTSA), are considered to be a viable alternative, due to their lower energy consumption and operating costs.

This work intends to design and simulate an industrial scale PTSA process capable of producing a methane stream with a purity higher than 99.995 % and replacing an existing multicolumn cryogenic distillation process. Surface equations (SE) were employed in the mathematical model of the process to calculate the thermodynamic properties of the mixture as a way to reduce the CPU time during the simulations.

The surface equations were developed by adjusting the values given by the REFPROP software package with the GERG-2008 as the equation of state (EoS). The values calculated with the SE present a maximum error of 18.7 %, 8.05 %, 15.7 %, 6.6 %, 14.8 % and 11.3 % for the density, viscosity, thermal conductivity, compressibility factor and heat capacities at constant pressure and volume, respectively, for mixtures with a molar fraction up to 55 % of CO_2.

The current simulation results showed that the entire replacement of an existing multicolumn cryogenic distillation process, which allows the reduction of a carbon dioxide concentration from 50.6 % to 50 ppm, by a PTSA process might not be feasible. Despite that, the last two columns of the distillation process can be replaced by a PTSA technology capable of reducing the carbon dioxide content from 10.6 % to 46 ppm, with a methane recovery of about 33.16 % and power consumption of 3.6 MW. However, the PTSA cycle presents a lower methane recovery when compared to the distillation process (33.16 % against 96.4 %).

Keywords: Natural gas upgrade; Pressure temperature swing adsorption; Thermodynamic surface equations; GERG-2008 EoS.

Resumo

A liquefação e o transporte de gás natural requerem um pré-tratamento para a remoção de impurezas, tal como azoto e dióxido de carbono, que podem danificar tubagens e equipamentos. Os processos de destilação criogénica de múltiplas colunas são usados para a produção de metano com um teor de dióxido de carbono inferior a 50 ppm, que é um dos requisitos para o transporte de gás natural liquefeito (GNL). Os processos de adsorção cíclicos, nomeadamente adsorção por modulação de pressão e temperatura (PTSA), são uma alternativa viável, devido ao menor consumo de energia e menores custos operacionais associados.

Este trabalho pretende projetar e simular um processo PTSA em escala industrial capaz de produzir metano com uma pureza superior a 99,995 %. As equações de superfície (SE) foram implementadas no modelo matemático do processo para calcular as propriedades termodinâmicas da mistura como forma de reduzir o tempo de CPU durante as simulações.

As equações de superfície foram obtidas através do ajuste dos valores fornecidos pelo *software* REFPROP, definindo o GERG-2008 como a equação de estado (EoS). Os valores calculados pelas SE apresentam um erro máximo de 18,7 %, 8,05 %, 15,7 %, 6,6 %, 14,8 % e 11,3 % para a massa volúmica, viscosidade, condutividade térmica, fator de compressibilidade e capacidade calorífica a pressão e volume constante, respetivamente, para misturas com uma fração molar até 55 % de CO_2.

Os resultados da simulação obtidos mostraram que a substituição total de um processo de destilação criogénica de múltiplas colunas, que permite a redução de uma concentração de dióxido de carbono de 50,6 % para 50 ppm, por um processo PTSA pode não ser viável. Apesar disso, as duas últimas colunas do processo de destilação podem ser substituídas por uma tecnologia PTSA capaz de reduzir o conteúdo de dióxido de carbono de 10,6 % para 46 ppm, com uma recuperação de metano de cerca de 33,16 % e um consumo de energia de 3,6 MW. No entanto, o ciclo PTSA apresenta uma menor recuperação de metano quando comparado ao processo de destilação (33,16 % contra 96,4 %).

Palavras-chave: Purificação de gás natural; adsorção por modulação de pressão e temperatura; equações de superfície termodinâmicas; GERG-2008 EoS.

Declaration

I hereby declare, under the word of honor, that this work is original and that all non-original contributions are indicated, and due reference is given to the author and source.

Mariana Carolina Nunes Bessa

(Mariana Carolina Nunes Bessa)

Porto, July 2020

Index

List of Figures

List of Tables

Notation and Glossary

a_p	particle specific area	m^{-1}
$b_{k,i}$	affinity constant	bar^{-1}
$b_{k,i,0}$	affinity constant at infinite temperature	bar^{-1}
$C_{g,i}$	bulk phase concentration of component *i*	mol m^{-3}
$C_{g,T}$	total bulk phase concentration	mol m^{-3}
C_p	gas mixture molar specific heat at constant pressure	J mol^{-1} K^{-1}
$\overline{C_p}$	average gas mixture specific heat at constant pressure	J mol^{-1} K^{-1}
$C_{p,i}$	molar specific heat of component *i* at constant pressure	J mol^{-1} K^{-1}
$\hat{C}_{p,s}$	solid specific heat at constant pressure (per mass unit)	J kg^{-1} K^{-1}
$\hat{C}_{p,w}$	wall specific heat at constant pressure (per mass unit)	J kg^{-1} K^{-1}
$C_{s,i}$	concentration of component *i* at the particle surface	mol m^{-3}
C_v	gas mixture molar specific heat at constant volume	J mol^{-1} K^{-1}
$C_{v,ads,i}$	molar specific heat of component *i* in the adsorbed phase at constant volume	J mol^{-1} K^{-1}
$C_{v,i}$	molar specific heat of component *i* at constant volume	J mol^{-1} K^{-1}
D_{ax}	axial dispersion coefficient	m^2 s^{-1}
D_m	molecular diffusivity	m^2 s^{-1}
d_p	particle diameter	m
d_{wi}	internal wall diameter	m
e	wall thickness	m
F_i	molar flow rate of component *i*	mol s^{-1}
F_{in}	inlet molar flow rate	mol s^{-1}
h_f	film heat transfer coefficient between the gas and particle	W K^{-1} m^{-2}
h_w	film heat transfer coefficient between the gas and wall	W K^{-1} m^{-2}
k	Boltzmann constant	J mol^{-1} K^{-1}
k_f	film mass transfer coefficient	m s^{-1}
k_g	gas mixture thermal conductivity	W m^{-1} K^{-1}
$k_{g,i}$	thermal conductivity of component *i*	W m^{-1} K^{-1}
$k_{h,i}$	homogeneous mass transfer coefficient of component *i*	s^{-1}
L	bed length	m
m_{ads}	adsorbent mass	kg
M_i	molecular weight of component *i*	kg mol^{-1}
M_{ij}	binary molecular weight of component *i* and *j*	g mol^{-1}
P	pressure	Pa
P_i	partial pressure of component *i*	bar
Pr	Prandtl number	
q_i	adsorbed concentration of component *i*	mol kg^{-1}
q_i^*	adsorbed concentration of component *i* in equilibrium with $C_{S,i}$	mol kg^{-1}
$q_{0,k,i}$	saturation capacity at infinite temperature	mol kg^{-1}
$\overline{q_{k,i}}$	averaged adsorbed concentration of component *i* for each site *k*	mol kg^{-1}
$q_{k,i}^*$	adsorbed concentration of component *i* in equilibrium with $C_{S,i}$ for each site *k*	mol kg^{-1}
$q_{sat,k,i}$	adsorption saturation capacity	mol kg^{-1}
Re	Reynolds number	
R_g	ideal gas constant	J mol^{-1} kg^{-1}

Sc	Schmidt number	
t	time	s
t_{bld}	blowdown step time	s
t_{cycle}	cycle time	s
t_{feed}	feed step time	s
t_{heat}	heating step time	s
t_{rinse}	rinse step time	s
T_0	reference temperature	K
T_g	bulk phase temperature	K
T_p	solid temperature	K
T_w	wall temperature	K
u_0	superficial velocity	m s^{-1}
y_i	bulk mole fraction of component *i*	
$y_{m,i}$	bulk mass fraction of component *i*	
z	axial position	m
Z	compressibility factor	
Z_i	compressibility factor of component *i*	

Greek Letters

α_w	ratio of the internal surface area to the volume of the column wall	m^{-1}
$-\Delta H_{k,i}$	enthalpic parameter for component *i* and each site *k*	J mol^{-1}
ΔT	temperature range of the system	K
ε	bed porosity	
ε_i	characteristic Lennard-Jones energy parameter of component *i*	J mol^{-1}
ε_{ij}	characteristic Lennard-Jones energy parameter for a binary mixture	J mol^{-1}
ε_p	particle porosity	
λ	heat axial dispersion coefficient	W m^{-1} K^{-1}
μ	gas mixture viscosity	Pa s
μ_i	viscosity of component *i*	Pa s
ρ	bulk gas mixture density	kg m^{-3}
ρ_{ap}	particle density	kg m^{-3}
ρ_b	bed density	kg m^{-3}
ρ_i	bulk density of component *i*	kg m^{-3}
ρ_w	wall density	kg m^{-3}
σ_i	characteristic Lennard-Jones length parameter of component *i*	Å
σ_{ij}	characteristic Lennard-Jones length parameter for a binary mixture	Å
$\chi_{k,i}$	parameter of the empirical correlation that relates $q_{sat,k,i}$ with T_p	
ω	acentric factor	
Ω_D	collision integral	

List of Acronyms

LNG	Liquified Natural Gas
PSA	Pressure Swing Adsorption
PTSA	Pressure Temperature Swing Adsorption
TSA	Temperature Swing Adsorption

1 Introduction

1.1 Framing and presentation of the work

Natural gas emerged as a cleaner energy source when compared to other petroleum-derivate fuels, capable of fulfilling the society's energy demands and reducing the carbon dioxide emissions. Impurities contained in natural gas, namely nitrogen and carbon dioxide, must be removed before its distribution via pipelines or as liquefied natural gas for long-distant transport to avoid corrosion on the pipelines and equipment.

Cryogenic distillation is one of the technologies available to reduce the carbon dioxide content in natural gas streams until the specifications required for its liquefaction and transport (< 50 ppm). Cyclic adsorptive processes are considered a viable alternative for the purification of natural gas when the final product is its liquified form, particularly pressure temperature swing adsorption (PTSA), which combines the pressure/vacuum and temperature swing adsorption methods. Lower energy requirements and operating costs are some of the advantages of this process.

One of the main goals of this thesis is to develop an industrial scale PTSA technology capable of producing a methane stream with a purity higher than 99.995 %. This unit would replace an existing cryogenic distillation process, where a natural gas stream with an initial carbon dioxide concentration of 50.6 % is treated in three sequential columns at cryogenic conditions.

The design and optimization of a PTSA unit, like any other cyclic process, takes a considerable amount of CPU time. So, ways to facilitate the simulation of the mathematical model used to describe the dynamic behavior of the process, should be pursued and employed in case they offer accurate information. Therefore, surface equations were developed to determine the thermodynamic properties of the mixture and implemented in the mathematical model as a way to reduce the time consumption during the process optimization.

1.2 Contribution of the author to the work

The basis of the model implemented on gPROMS ModelBuilder was already established. The transport parameters were added to the model in the present work, as a function of time and position within the column, as well as additional steps of the PTSA process.

Furthermore, the surface equations for the compressibility factor and the heat capacity at constant pressure and volume were already obtained by a previous study. In this work, the

surface equations for the density, viscosity, and thermal conductivity were developed and written in the model of the program as a function of time and position in the column.

1.3 Organization of the thesis

This work is divided into five main parts.

The context and description of the key concepts involved in this work are presented in chapter 1.

In chapter 2, an introduction about natural gas and its main applications, purification technologies and distribution methods are presented. Pressure temperature swing adsorption, which is one of the purification processes used for the removal of carbon dioxide from natural gas streams to produce high purity liquified natural gas, is detailed in this chapter. The description of the thermodynamic calculation method used to speed the process simulations is also included in this chapter.

Chapter 3 details the mathematical model used to describe the dynamic behavior of the PTSA process. The computational aspects are also presented in this chapter, which includes the main concepts of the modeling program, and the calculation procedure adopted for the optimization of the process.

In chapter 4, the fixed bed and simulation results are presented, as well as the proposed pressure temperature swing adsorption process. The polynomial equations developed to determine the thermodynamic properties of the mixture are also included in this chapter.

Lastly, the main conclusions, suggestions for future work, and the assessment of the work done in this thesis are presented in chapters 5 and 6.

2 Context and State of the art

2.1 Natural gas

Natural gas has emerged in the last two decades as a promising fuel to replace coal and oil worldwide. The increase in natural gas demand was driven by the growing concern with the energy sustainability for the future generation, as well as with the adverse impact of greenhouse gases (GHG) on the global climate (Mokhatab et al., 2019).

As a matter of fact, natural gas emits less carbon dioxide than other petroleum-derivate fuels, when burned: around 45 % and 30 % less than coal and oil, respectively (Campo et al., 2016). Additionally, it presents a lower sulfur content, and no particles are released during combustion, which makes it a cleaner fuel (Vikse et al., 2018).

Natural gas is composed by methane (typically, 87-97 %), heavier hydrocarbons, such as ethane, propane, butanes and pentanes, and also carbon dioxide, helium, hydrogen sulfide, and nitrogen. However, its composition may differ significantly depending on the reservoir from which the gas was extracted (Viswanathan, 2016). This fossil energy is widely used as a fuel, as a feedstock for petrochemicals, such as fertilizers and dyes, and to generate heat and electric power. In natural gas power plants, the electricity is mostly generated in gas turbines through the use of the hot exhaust gases produced during the combustion process (Speight, 2018).

The delivery of natural gas to consumers is traditionally made via pipelines or as a Liquefied Natural Gas (LNG) for long-distance transport. LNG has a specific volume of about 600 times lower than the natural gas at STP conditions, enabling its transport by cargo ships and trucks, which are more economically attractive than pipelines. Furthermore, the LNG technology makes natural gas available in the global market, allowing its supply in places where the construction of pipeline networks and underground natural gas storage systems would be technical and politically infeasible (Mokhatab et al., 2019).

LNG plants are capital-intensive primarily as a result of high energy consumption and use of expensive cryogenic material to cool down the natural gas to approximately −162°C, at atmospheric pressure. However, more energy-efficient liquefaction methods are currently being studied, since this process embodies around 30-40 % of the overall costs, and so advances in this area can be expected in the forthcoming years (Mokhatab et al., 2019; Vikse et al., 2018).

The natural gas upgrade is an essential step before its distribution to remove impurities like carbon dioxide and nitrogen not only to enhance this fuel energy content but also to prevent

corrosion in pipelines and equipment. According to the pipeline quality standards, the upper limit for nitrogen and carbon dioxide is typically 4 % and 2 %, respectively. The presence of carbon dioxide (above 50 ppm) in LNG plants represents a major problem, since it can form dry ice inside the pipeline networks causing transportation drawbacks. Therefore, the separation of carbon dioxide from natural gas streams is of vital importance (Berstad et al., 2012; Shimekit et al., 2012).

Absorption, membrane, adsorption, and cryogenic distillation processes are examples of the several technologies available for the CO_2/CH_4 separation. For the transport of LNG, cryogenic distillation is a suitable technology to reduce carbon dioxide to ppm levels from sizeable natural gas volumes (Berstad et al., 2012). However, cyclic adsorption processes, such as pressure temperature swing adsorption (PTSA), at almost cryogenic conditions, have been presented as a cost-effective alternative to produce high purity LNG, due to their smaller energy consumption and lower operating costs (Moreira et al., 2017).

2.2 Pressure Temperature Swing Adsorption

Adsorptive processes are based on the selective adsorption of one or more components of a fluid mixture in the surface of a solid adsorbent by differences in equilibrium isotherms, differences in the mass transport kinetics, or steric effects (Yang, 1987).

The gas-adsorption applications are divided into two categories: purification and bulk separation. Drying of air and carbon dioxide removal from ethylene and natural gas are some of the commercial purification processes. The bulk separation processes include the production of oxygen and nitrogen from the air and the separation of *n*-paraffins from *i*-paraffins and aromatics (Yang, 1987).

The choice of the adsorbent is one of the most critical aspects in the design of any adsorption process. Activated carbon, metal-organic frameworks (MOFs), carbon molecular sieves and zeolites are some of the adsorbents use in the CO_2/CH_4 separation (Pour et al., 2015). Zeolites, which are porous crystalline aluminosilicates with frameworks made of SiO_4 and AlO_4 tetrahedra linked through shared oxygen atoms (Ruthven, 1984), present numerous advantages, for instance, high thermal stability, high surface area, cheapness, and simple ion exchange, particularly the synthetic ones, such as A, X, ZSM-5, beta, and Y (Pour et al., 2015).

Cyclic adsorption processes operate with multiple packed beds that alternate between two main steps: adsorption, where the adsorbent retains the heavier components contained in the gas mixture, and regeneration when those same species are removed from the adsorbent. The regeneration method is commonly made by pressure or thermal swing. In temperature swing adsorption (TSA) units, the adsorbent is regenerated by increasing the

bed temperature through a preheated gas. In contrast, the regeneration in pressure or vacuum swing adsorption (PSA/VSA) systems is accomplished by reducing the total bed pressure (Yang, 1987).

The combination of the PSA and TSA methods originates the so-called pressure temperature swing adsorption process, which presents several advantages like the reduction of energy consumption, an increase in the efficiency of the process, and a decrease in the total costs. In PTSA units, the operating cost can be reduced by using lower regeneration temperatures than those required in TSA systems (R. K. Zhao et al., 2018).

PTSA systems are applied in numerous purification processes, for instance, production of high purity natural gas streams with the removal of CO_2 and/or H_2S (Kamakoti, 2014), separation of heavy hydrocarbons from natural gas streams (Ravikovitch, 2014), and removal of toxic contaminants from the air (Malik, 1994). Recent studies have shown the potential of the hybridization of solar energy in fossil fuel-based power plants that used solar-assisted pressure-temperature swing adsorption (SOL-PTSA) for CO_2 capture and storage (CCS). The integration of solar energy for adsorbent regeneration can reduce carbon emissions and improve the efficiency of power plants. However, the information available in the literature regarding the SOL-PTSA technology is limited (R. K. Zhao et al., 2019; R. K. Zhao et al., 2018).

A PTSA cycle comprises several sequential steps that occur inside the bed, mainly pressurization, feed, blowdown, heating, and cooling. In the feed step, the heavier component(s) of the gas stream is(are) adsorbed in the packed bed and, consequently, an enriched stream with the lighter component(s) is produced at high pressure and low temperature. This is followed by the blowdown and heating steps, where the column is regenerated by reducing the bed pressure and increasing the temperature, respectively, which results in the production of a stream composed by the desorbed heavier component(s). After the regeneration, the column is cooled down by passing a fluid, such as cooling water, and then pressurized with the feed stream (Carmo, 2018; R. Zhao et al., 2017). The separation continues until a cyclic steady state (CSS) is achieved.

Pressure equalization and rinse steps are commonly added in cyclic processes as a way to decrease the energy consumption of the system and/or to improve the product recovery. The rinse step consists in passing the stream enriched with the heavier component(s) through the bed before blowdown (Ferreira et al., 2015). The simulation of cyclic adsorptive processes is more demanding as the complexity of the model that describes the dynamic behavior of adsorption increases. So, to reduce simulation time consumption, simplifications in the model should be employed without compromising the reliability of the results (Ribeiro et al., 2008).

2.3 Thermodynamic surface equations

Thermodynamic properties of fluids can be calculated with equations of state (EoS) over a wide range of pressure, temperature, and mixture composition. An EoS must be easy to implement and predict the fluid properties accurately to minimize errors in process simulations (Rowland et al., 2016).

The Groupe Européen de Recherches Gazières (GERG) 2008 EoS is an ISO standard reference equation (ISO 20765-2/3) suitable for natural gas applications (Varzandeh et al., 2017). It is explicit in the Helmholtz free energy as a function of density, temperature and composition. It describes accurately the thermodynamic properties of pure components of natural gas and their mixtures over the gas phase, liquid phase, supercritical region, and vapor-liquid equilibrium states. The range of validity is temperatures from 60 to 700 K and pressures up to 70 MPa (Rowland et al., 2016).

The GERG-2008 EoS is based on experimental thermodynamic data of twenty-one components of natural gas: methane, ethane, propane, *n*-butane, *i*-butane, *n*-pentane, *i*-pentane, *n*-hexane, *n*-heptane, *n*-octane, *n*-nonane, *n*-decane, hydrogen, helium, nitrogen, oxygen, argon, water, carbon monoxide, carbon dioxide, and hydrogen sulfide. The experimental measurements of the binary mixtures formed with these components are also incorporated in this model (Kunz et al., 2012).

Compared with classical EoS used in the oil and gas industries, such as Peng-Robinson, Redlich-Kwong, and Soave-Redlich-Kwong, the GERG-2008 EoS has advantages in the calculation of phase equilibrium and physical properties of natural gas-related systems, particularly in the prediction of density, saturated liquid density, compressibility, heat capacity, and Joule-Thomson coefficient of pure (Varzandeh et al., 2017). Varzandeh et al. (2017) have found that Soave-BWR shows a better performance in bubble point pressure and vapor phase composition predictions of binary mixtures than GERG-2008, despite leading to more imprecise descriptions of the fluid properties in general.

In previous studies, GERG-2008 EoS property packages, such as REFPROP (REFerence fluid PROPerties), developed by NIST (National Institute of Standards and Technology), were incorporated in simulating environments through the use of the Computer-Aided Process Engineering standard (CAPE-OPEN). This interface allows the communication and exchange of information (pressure, temperature, composition, …) between process modeling environments, like Aspen Plus and Aspen HYSYS of AspenTech and gPROMS of Process Systems Enterprise, and external components (Dauber et al., 2012). Although the integration of the GERG-2008 EoS property package in modeling programs through the CAPE-OPEN interface

leads to satisfactory thermodynamic predictions for natural gas applications, it also requires a high amount of CPU time (Moreira et al., 2017).

Moreira et al. (2017) have shown that the use of polynomial equations as an alternative calculation method to determine some of the fluids thermodynamic properties, namely compressibility factor and heat capacities at constant volume and pressure, leads to similar results of those obtained using a GERG-2008 EoS property package incorporated in a given modeling tool, but with a much lower computational time. These authors had reported that the breakthrough curve simulations for the adsorption step took about 20.5 h to be completed when the compressibility factor and heat capacities at constant volume and pressure were obtained using the GERG-2008 EoS, and only 111 s when the thermodynamic calculation method for these thermodynamic properties was done with polynomial equations. Therefore, the implementation of thermodynamic polynomial equations (also named surface equations (SE) throughout this work) is an excellent method to simplify the process model.

3 Methods

3.1 Mathematical model

The dynamic behavior of adsorption in a packed bed is represented through a mathematical model that must include mass, energy, and momentum balances (Da Silva et al., 1999). The development of the mathematical model to be employed in this work was based on the following assumptions:

- **real gas behavior**;
- axial dispersed flow;
- external mass and heat transfer resistances expressed with the film model;
- particle mass transfer resistance expressed with the Linear Driving Force (LDF) model;
- no temperature gradients inside each particle, as the heat transfer in the solid phase is much faster than in the gas phase;
- the column wall interchanges energy with the gas phase inside the column but not with the external environment - adiabatic operation;
- constant porosity along the bed;
- the Ergun equation is valid locally.

The material balance for each component in the gas phase is given by:

$$\frac{\partial}{\partial z}\left(\varepsilon D_{ax} C_{g,T} \frac{\partial y_i}{\partial z}\right) - \frac{\partial}{\partial z}\left(u_0 C_{g,i}\right) - \varepsilon \frac{\partial C_{g,i}}{\partial t} - (1-\varepsilon) a_p k_f \left(C_{g,i} - C_{s,i}\right) = 0 \qquad (1)$$

where z is the axial position, ε is the bed porosity, D_{ax} is the mass axial dispersion coefficient, $C_{g,T}$ and $C_{g,i}$ are, respectively, the total and component i gas phase concentrations, y_i is the molar fraction of component i, u_0 is the superficial velocity, t is the time, a_p is the particle external specific area, k_f is the film mass transfer coefficient, and $C_{s,i}$ is the concentration of component i at the solid interface.

The energy balance in the gas phase is described by:

$$\begin{aligned} \frac{\partial}{\partial z}\left(\lambda \frac{\partial T_g}{\partial z}\right) - u_0 C_{g,T} C_p \frac{\partial T_g}{\partial z} + \varepsilon Z R_g T_g \frac{\partial C_{g,T}}{\partial t} - (1-\varepsilon) a_p h_f \left(T_g - T_p\right) \\ - \frac{4 h_w}{d_{wi}} \left(T_g - T_w\right) - \varepsilon C_{g,T} C_v \frac{\partial T_g}{\partial t} = 0 \end{aligned} \qquad (2)$$

where λ is the heat axial dispersion coefficient, T_g, T_p, and T_w are the gas phase, solid phase, and wall temperatures, respectively, C_p is the heat capacity of the mixture at constant

pressure, Z is the compressibility factor, R_g is the universal gas constant, h_f is the heat transfer coefficient between the gas and the particle, h_w is the heat transfer coefficient between the gas phase and the column wall, d_{wi} is the internal wall diameter, and C_v is the heat capacity of the mixture at constant volume.

The momentum balance is given by the Ergun equation:

$$-\frac{\partial P}{\partial z} = \frac{150\mu(1-\varepsilon)^2}{\varepsilon^3 d_p^2}u_0 + \frac{1.75(1-\varepsilon)\rho}{\varepsilon^3 d_p}u_0|u_0| \quad (3)$$

where P is the pressure, d_p is the particle diameter, and ρ is the gas density.

The gas-phase cannot be considered an ideal gas for the operating conditions under study (temperatures between 206 and 473 K, pressures up to 70 bar). Thus, the behavior of the real gas is written by:

$$P = ZC_{g,T}R_gT_g \quad (4)$$

The Linear Driving Force model (LDF) can be used to characterize the mass transfer rates inside the adsorbent particle, being the material balance in the solid phase given by:

$$\frac{\partial \overline{q_{k,i}}}{\partial t} = k_{h,i}(q^*_{k,i} - \overline{q_{k,i}}) \quad (5)$$

where $k_{h,i}$ is the homogeneous mass transfer coefficient of component *i*, $\overline{q_{k,i}}$ is the particle averaged adsorbed concentration of component *i* for each adsorption site *k*, and $q^*_{k,i}$ is the adsorbed concentration of component *i* in equilibrium with $C_{s,i}$ for each adsorption site *k*.

q^*_i is determined by the multicomponent extension of the Dual Site Langmuir (DSL) isotherm:

$$q^*_i = \sum_{k=1,2} q^*_{k,i} = \sum_{k=1,2} q_{sat,k,i}\frac{b_{k,i}P_i}{1+\sum_{j=1}^{n} b_{k,j}P_j} \quad (6)$$

where $q_{sat,k,i}$ is the adsorption saturation capacity for each site *k* for component *i*, $b_{k,i}$ is the affinity constants of component *i* for each adsorption site *k*, and P_i is the partial pressure of component *i*. This adsorption equilibrium model assumes that the adsorbent surface is heterogeneous and considers two different types of adsorption sites. The parameters $q_{sat,k,i}$ are calculated by Eq. (7), whereas $b_{k,i}$ are determined by Eq. (8) (Do, 1998):

$$q_{sat,k,i} = q_{0,k,i}\exp\left[\chi_{k,i}\left(1-\frac{T_p}{T_0}\right)\right] \tag{7}$$

$$b_{k,i} = b_{0,k,i}\exp\left(\frac{-\Delta H_{ads,k,i}}{R_g T_p}\right) \tag{8}$$

where $q_{0,k,i}$ and $b_{0,k,i}$ are the adsorption saturation capacity and the affinity constant at infinite temperature, respectively, $\chi_{k,i}$ is a dimensionless constant, and $(-\Delta H_{ads,k,i})$ is an enthalpic parameter related with heat of adsorption for component *i* and each site *k*. As for T_0, this represents the reference temperature.

Equaling the fluxes at the particle surface:

$$\frac{a_p k_f}{\rho_{ap}}\left(C_{g,i}-C_{s,i}\right) = k_{h,i}\sum_{k=1,2}\left(q^*_{k,i}-\overline{q_{k,i}}\right) \tag{9}$$

where ρ_{ap} is the particle density.

An overall energy balance of the gas phase, adsorbed phase and the solid phase inside a particle is given by:

$$\begin{aligned}(1-\varepsilon)\left[\rho_{ap}\sum_{i=1}^{n}\sum_{k=1,2}\overline{q_{k,i}}\,C_{v,ads,i}+\rho_{ap}\hat{C}_{p,s}\right]\frac{\partial T_p}{\partial t}\\ = \rho_b\sum_{i=1}^{n}\sum_{k=1,2}(-\Delta H_{ads,k,i})\ \frac{\partial\overline{q_{k,i}}}{\partial t}+(1-\varepsilon)a_p h_f\left(T_g-T_p\right)\end{aligned} \tag{10}$$

where $C_{v,ads,i}$ is the molar specific heat of component *i* in the adsorbed phase at constant volume, and $\hat{C}_{p,s}$ is the solid specific heat at constant pressure per mass unit. The molar specific heat of the adsorbed gas is assumed to be equal to the one in the gas (Da Silva, 1999), while the solid specific heat per mass unit for the binderless zeolite 13 X is expressed by the following equation (Qiu et al., 2000):

$$\hat{C}_{p,s} = -0.0062{T_P}^2 + 5.2124T_p - 69.73 \tag{11}$$

The energy balance to the column wall assumes energy exchange with the gas phase inside the column, but not with the external environment, and is written by:

$$\rho_w \hat{C}_{p,w} \frac{\partial T_w}{\partial t} = \alpha_w h_w (T_g - T_p) \quad (12)$$

where ρ_w is the wall density, $\hat{C}_{p,w}$ is the wall specific heat at constant pressure per mass unit, and α_w is the ratio of internal surface area to the column wall volume, that is calculated by:

$$\alpha_w = \frac{d_{wi}}{e(d_{wi} + e)} \quad (13)$$

where e is the wall thickness.

Considering that the pressure is controlled at the end of the column, initially filled with a given composition, the initial and boundary conditions required to solve the system of partial differential equations of an adsorption fixed bed are presented in Table 1.

Table 1 - Initial and boundary conditions of the adsorption fixed bed model.

Initial conditions	Boundary conditions	
y_i = initial conditions	z=0, inlet	z=L, outlet
$\frac{\partial q_i}{\partial t}$ =0	$u_{0inlet} C_{inlet,i} = u_0 C_{g,i} - \varepsilon D_{ax} C_{g,T} \frac{\partial y_i}{\partial z}$	$\frac{\partial C_{g,i}}{\partial z}$ =0
T_g=T_p=T_w=T_{inlet}	$u_{0inlet} C_{inlet,T} = u_0 C_{g,T}$	P=P_{exit}
	$u_{0inlet} C_{inlet,i} C_p T_{inlet} = u_0 C_{g,T} C_p T_g - \lambda \frac{\partial T_g}{\partial z}$	$\frac{\partial T_g}{\partial z}$=0

The transport and thermodynamic parameters must be defined to complete the mathematical model. Thereby, the Wakao and Funazkri correlations are used to calculate the axial mass and heat dispersions coefficients and the mass and heat transfer coefficients (Yang, 1987):

$$\frac{\varepsilon D_{ax}}{D_m} = 20 + 0.5 Sc\, Re \quad (14)$$

$$\frac{\lambda}{k_g} = 7 + 0.5 \,\mathrm{Pr}\, Re \quad (15)$$

$$\frac{k_f d_p}{D_m} = 2.0 + 1.1 Re^{0.6} Sc^{1/3} \quad (16)$$

$$\frac{h_f d_p}{k_g} = 2.0 + 1.1 Re^{0.6} Pr^{1/3} \quad (17)$$

valid for 3 < Re < 10000. D_m is the molecular diffusivity, Sc and Re are the Schmidt and Reynolds numbers, respectively, k_g is the thermal conductivity of the gas and Pr is the Prandtl number.

The molecular diffusivity is obtained by the Chapman-Enskog (Prausnitz, 2001):

$$D_m = \frac{2.66 \times 10^{-2} {T_g}^{3/2}}{P {M_{ij}}^{1/2} {\sigma_{ij}}^2 \Omega_D} \quad (18)$$

where M_{ij} is the binary molecular weight of component *i* and *j*, Ω_D is the collision integral and σ_{ij} is the characteristic Lennard-Jones length parameter, that is given by:

$$\sigma_{ij} = \frac{\sigma_i + \sigma_j}{2} \quad (19)$$

where σ_i and σ_j are the characteristic Lennard-Jones length parameter for each component. The binary molecular weight of component *i* and *j* is calculated by (Prausnitz, 2001):

$$M_{ij} = 2000 \left[\frac{1}{M_i} + \frac{1}{M_j}\right]^{-1} \quad (20)$$

where M_i and M_j are the molecular weight of components *i* and *j*, respectively. The collision integral is calculated by (Prausnitz, 2001):

$$\Omega_D = \frac{1.06036}{\omega^{0.15\ 610}} + \frac{0.19300}{\exp(0.47635\omega)} + \frac{1.03587}{\exp(1.52996\omega)} + \frac{1.76474}{\exp(3.89411\omega)} \quad (21)$$

where the acentric factor (ω) is given by:

$$\omega = \frac{kT_g}{\varepsilon_{ij}} \quad (22)$$

with k being the Boltzmann constant and ε_{ij} being the characteristic Lennard-Jones energy, which is calculated by:

$$\frac{\varepsilon_{ij}}{k} = \frac{\sqrt{\varepsilon_i \varepsilon_j}}{k} \quad (23)$$

where σ_i and σ_j are the characteristic Lennard-Jones energy parameter for each component. The characteristic Lennard-Jones length and energy for each component are presented in Table 2 (Bird, 2002):

Table 2 - Characteristic Lennard-Jones parameters for each component.

Component	σ_i (Å)	ε_i/k (K)
CH_4	3.780	154
CO_2	3.996	190

The homogeneous mass transfer coefficients of the gases under study are estimated by the following expressions, which were developed using the binderless zeolite 13X as the adsorbent (Moreira et al., 2017):

$$k_{h,CO_2} = 1.4 \times 10^{-4}\, e^{1.7\times10^{-2}\, T_P} \tag{24}$$

$$k_{h,CH_4} = 2.7 \times 10^{-4}\, e^{1.4\times10^{-2}\, T_P} \tag{25}$$

The convective heat transfer coefficient between the gas and the wall is calculated with the Wasch and Froment correlation (Da Silva, 1999):

$$\frac{h_w d_{wi}}{k_g} = 140 + 0.013396 \frac{{d_{wi}}^2}{d_p k_g} Re \tag{26}$$

Fluid thermodynamic properties are described by polynomial/surface equations in the mathematical model of the proposed process. The density, viscosity, and thermal conductivity values of the gases in this study were calculated with the GERG-2008 EoS using the REFPROP software package (version 9.1) and then fitted to SE. At the same time, the compressibility factor and heat capacities at constant volume and pressure values are estimated using the SE developed by Moreira et al. (2017) (see section 4.1).

3.2 PTSA cycle

The modeling of a PTSA cycle involves the same equations presented in the previous section for an adsorption fixed bed. The boundary conditions for each step of the proposed PTSA process are given in Table 3. The pressure is controlled at the outlet (P_{exit}); indeed the pressure during equalization-depressurization and blowdown steps is considered to decrease exponentially with time as to represent the behavior of a valve.

Table 3 - Boundary conditions for the PTSA cycle.

Co-current pressurization with feed	
z=0, inlet	z=L
$u_0 C_{g,i} - \varepsilon D_{ax} C_{g,T} \frac{\partial y_i}{\partial z} = u_{0inlet} C_{inlet,i}$	$\frac{\partial C_{g,i}}{\partial z}$ =0
$u_{0inlet} C_{inlet,T} = u_0 C_{g,T}$	u_0=0
$u_0 C_{g,T} C_p T_g - \lambda \frac{\partial T_g}{\partial z} = u_{0inlet} C_{inlet,i} C_p T_{inlet}$	$\frac{\partial T_g}{\partial z}$=0
Pressure equalization-depressurization	
z=0	z=L, outlet
$\frac{\partial C_{g,i}}{\partial z}$ =0	$\frac{\partial C_{g,i}}{\partial z}$=0
u_0=0	$P = P_{exit}$
$\frac{\partial T_g}{\partial z}$=0	$\frac{\partial T_g}{\partial z}$=0
Feed/Rinse	
z=0, inlet	z=L, outlet
$u_0 C_{g,i} - \varepsilon D_{ax} C_{g,T} \frac{\partial y_i}{\partial z} = u_{0inlet} C_{inlet,i}$	$\frac{\partial C_{g,i}}{\partial z}$ =0
$u_{0inlet} C_{inlet,T} = u_0 C_{g,T}$	$P = P_{exit}$
$u_0 C_{g,T} C_p T_g - \lambda \frac{\partial T_g}{\partial z} = u_{0inlet} C_{inlet,i} C_p T_{inlet}$	$\frac{\partial T_g}{\partial z}$=0
Blowdown	
z=0, outlet	z=L
$\frac{\partial C_{g,i}}{\partial z}$ =0	$\frac{\partial C_{g,i}}{\partial z}$ =0
$P = P_{exit}$	u_0=0
$\frac{\partial T_g}{\partial z}$=0	$\frac{\partial T_g}{\partial z}$=0
Heating	
z=0, outlet	z=L, inlet
$P = P_{exit}$	$u_0 C_{g,i} - \varepsilon D_{ax} C_{g,T} \frac{\partial y_i}{\partial z} = u_{0inlet} C_{inlet,i}$
$\frac{\partial C_{g,i}}{\partial z}$ =0	$u_{0inlet} C_{inlet,T} = u_0 C_{g,T}$
$\frac{\partial T_g}{\partial z}$=0	$u_0 C_{g,T} C_p T_g - \lambda \frac{\partial T_g}{\partial z} = u_{0inlet} C_{inlet,i} C_p T_{inlet}$

Pressure equalization-pressurization	
z=0, inlet	z=L
$u_0 C_{g,i} - \varepsilon D_{ax} C_{g,T} \frac{\partial y_i}{\partial z} = u_{0inlet} C_{inlet,i}$	$\frac{\partial C_{g,i}}{\partial z}$ =0
$u_{0inlet} C_{inlet,T} = u_0 C_{g,T}$	u_0=0
$u_0 C_{g,T} C_p T_g - \lambda \frac{\partial T_g}{\partial z} = u_{0inlet} C_{inlet,i} C_p T_{inlet}$	$\frac{\partial T_g}{\partial z}$=0

The performance of a cyclic adsorption process is typically measured according to product purity, product recovery, and adsorbent productivity (Ferreira et al., 2015). These parameters are given by Eqs. (27)-(29), respectively, for the methane product (the lighter component of the CO_2/CH_4 mixture):

$$CH_4\ purity = \frac{\int_0^{t_{feed}} F_{CH_4,out}\,dt + \int_0^{t_{rinse}} F_{CH_4,out}\,dt}{\sum_{i=1}^{n} \int_0^{t_{feed}} F_{i,out}\,dt + \sum_{i=1}^{n} \int_0^{t_{rinse}} F_{i,out}\,dt} \quad (27)$$

$$CH_4\ recovery = \frac{\int_0^{t_{feed}} F_{CH_4,out}\,dt + \int_0^{rinse} F_{CH_4,out}\,dt - \int_0^{t_{heat}} F_{CH_4,in}\,dt}{\int_0^{t_{feed}} F_{CH_4,in}\,dt} \quad (28)$$

$$CH_4\ productivity\ (mol\ kg^{-1}\ h^{-1}) = \frac{\int_0^{t_{feed}} F_{CH_4,in}\,dt}{m_{ads} \frac{t_{cycle}}{3600}} \times CH_4\ recovery \quad (29)$$

where t_{feed}, t_{rinse}, and t_{heat} are the adsorption, rinse, and heating step times, respectively, F_i is the molar flow rate of each component, m_{ads} is the adsorbent mass, and t_{cycle} is the cycle time. The CH_4 purity can also be described in terms of the CO_2 content (in ppm):

$$CO_2\ content\ (ppm) = \frac{\int_0^{t_{feed}} F_{CO_2,out}\,dt + \int_0^{t_{rinse}} F_{CO_2,out}\,dt}{\sum_{i=1}^{n} \int_0^{t_{feed}} F_{i,out}\,dt + \sum_{i=1}^{n} \int_0^{t_{rinse}} F_{i,out}\,dt} \times 10^6 \quad (30)$$

The purity and recovery of the heavy product are given by Eqs. (31)-(32), respectively:

$$CO_2\ purity = \frac{\int_0^{t_{bld}} F_{CO_2,out}\,dt + \int_0^{t_{heat}} F_{CO_2,out}\,dt}{\sum_{i=1}^{n} \int_0^{t_{bld}} F_{i,out}\,dt + \sum_{i=1}^{n} \int_0^{heat} F_{i,out}\,dt} \quad (31)$$

$$CO_2\ recovery = \frac{\int_0^{t_{bld}} F_{CO_{2,out}} dt + \int_0^{t_{heat}} F_{CO_{2,out}} dt - \int_0^{t_{rinse}} F_{CO_{2,in}} dt}{\int_0^{t_{feed}} F_{CO_{2,in}} dt} \quad (32)$$

where t_{bld} is the blowdown step time.

The power consumption of the process is obtained by Eq. (33), considering the adiabatic compression and cooling of part of the heavy product, which is used for the rinse step:

$$Power\ Consumption\ (W) = F_{in,heat} \overline{C}_{p,heat}\, \Delta T \frac{2t_{heat}}{t_{cycle}} + \frac{1}{\eta} F_{in,rinse} R_g T_{in} Z_{in} \frac{\gamma}{\gamma - 1} \left[\left(\frac{P_{out}}{P_{in}} \right)^{(\gamma-1)/\gamma} - 1 \right] + F_{in,rinse} \overline{C}_{p,bld+heat}\, \Delta T \quad (33)$$

where $F_{in,heat}$ and $F_{in,rinse}$ are the inlet molar flow rate used in the heating and rinse steps, respectively, $\overline{C}_p$ is the average gas mixture specific heat at constant pressure, ΔT is the temperature range of the system, η is the efficiency of the adiabatic compression, and γ is the ratio between the heat capacity of the gas mixture at constant pressure and the heat capacity of the gas mixture at constant volume.

3.3 Computational aspects

The design and simulation of an industrial scale PTSA process were done using the gPROMS ModelBuilder (version 5.1.1). This program allows the implementation and numerical resolution of the obtained system of partial differential and algebraic equations (IPDAEs) that integrates the mathematical model used to define the proposed process. The system of IPDAEs are solved using a discretization method for distribution domains that reduce the problem to the solution of a set of DAEs ("PSE: Products - Gproms - Custom Modeling," 2020). The orthogonal collocation in finite elements method (OCFEM) was the one used in the simulations.

The modeling of the process requires the definition of the case study, which includes establishing the operating conditions and process specifications and the sizing of the bed (diameter, length, and porosity). Fixed bed simulations are run to determine the feed time, as well as to comprehend the dynamic behavior of adsorption throughout the packed column. The dynamic optimization is made until a cyclic steady state is achieved. The performance of the system at CSS is then analyzed, and if the results are not satisfactory, a new cycle is simulated with different set of parameter values, such as feed time or inlet molar flow rate used in the feed and heating steps. This iterative process is done until the “optimal” process is found.

Figure 1 represents the calculation procedure for the optimization of the process:

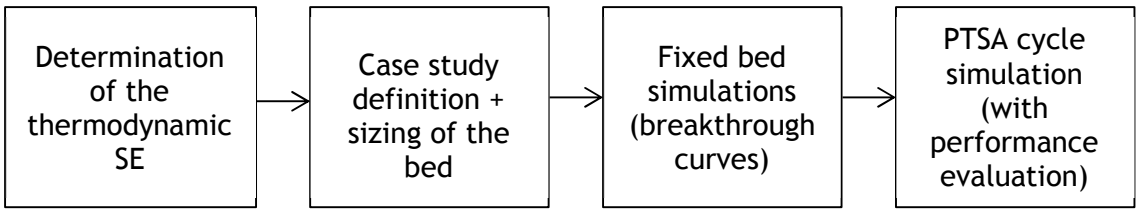

Figure 1 – Calculation procedure for the optimization of the process.

The surface equations implemented in the model to determine the density, viscosity, and thermal conductivity of a mixture, at a specific time and position in the column, were obtained using the software MATLAB, where the sum of the quadratic errors between the values determined with the SE and the ones obtained with the GERG-2008 EoS was defined as the objective function to be minimized. As mentioned before, the calculation of the compressibility factor and heat capacities at constant volume and pressure was done using the SE developed by a previous study.

4 Results and discussion

4.1 Fluid thermodynamic properties

In this work, the density, viscosity, and thermal conductivity surface equations, which are presented in Table 4, were obtained for CH_4 and CO_2 as pure components at a temperature range between 180 and 480 K and pressures from 0.1 to 80 bar.

Table 4 - Density, viscosity, and thermal conductivity surface equations for pure components.

$\rho_i = a + \frac{b}{T_g} + cP + d\frac{P}{T_g} + e\frac{P^2}{T_g} + f\frac{P}{{T_g}^2} + g\frac{P^3}{{T_g}^2} + h\frac{P^2}{{T_g}^3} + i\frac{P^2}{{T_g}^2} + j\frac{P^3}{{T_g}^3}$
$\mu_i = a + bT_g + cP + dP^2 + eT_gP$
$k_{g,i} = a + bT_g + cP + d{T_g}^2 + eT_gP + fP^2 + gT_gP^2$

The SE parameters *a* to *j* were adjusted to minimize the errors between the values calculated with the REFPROP software defining the GERG-2008 as the EoS and the ones determined by the SE. The SE parameters are presented in Table 5 for each component.

Table 5 - Parameters of the SE for the density, viscosity, and thermal conductivity.

Thermodynamic property	SE Parameter	CH_4	CO_2
Density	a (kg m^{-3})	-7.21×10^{-5}	-7.64×10^{-4}
	b (kg K m^{-3})	0.030	0.25
	c (kg m^{-3} Pa^{-1})	-9.17×10^{-8}	-1.39×10^{-7}
	d (kg K m^{-3} Pa^{-1})	0.00199	0.00540
	e (kg K m^{-3} Pa^{-2})	1.03×10^{-10}	7.20×10^{-10}
	f (kg K^2 m^{-3} Pa^{-1})	-0.00826	-0.0180
	g (kg K^2 m^{-3} Pa^{-3})	-2.39×10^{-15}	-2.31×10^{-14}
	h (kg K^3 m^{-3} Pa^{-2})	1.70×10^{-5}	1.33×10^{-4}
	i (kg K^2 m^{-3} Pa^{-2})	-7.81×10^{-8}	-5.83×10^{-7}
	j (kg K^3 m^{-3} Pa^{-3})	7.78×10^{-13}	9.68×10^{-12}

Viscosity	a (Pa s)	$1.15x10^{-6}$	$5.96x10^{-7}$
	b (Pa s K^{-1})	$3.28x10^{-8}$	$4.78x10^{-8}$
	c (s)	$5.44x10^{-13}$	$6.86x10^{-13}$
	d (s Pa^{-1})	$1.90x10^{-20}$	$3.73x10^{-20}$
	e (s K^{-1})	$-1.38x10^{-15}$	$-1.86x10^{-15}$
Thermal conductivity	a (W m^{-1} K^{-1})	0.011	-0.002
	b (W m^{-1} K^{-2})	$9.75x10^{-6}$	$4.64x10^{-5}$
	c (W m^{-1} K^{-1} Pa^{-1})	$1.96x10^{-9}$	$1.08x10^{-9}$
	d (W m^{-1} K^{-3})	$2.16x10^{-7}$	$5.17x10^{-8}$
	e (W m^{-1} K^{-2} Pa^{-1})	$-4.07x10^{-12}$	$-2.12x10^{-12}$
	f (W m^{-1} K^{-1} Pa^{-2})	$1.60x10^{-16}$	$2.62x10^{-16}$
	g (W m^{-1} K^{-2} Pa^{-2})	$-3.52x10^{-19}$	$-5.17\ x10^{-19}$

The density, viscosity, and thermal conductivity values given by the GERG-2008 EoS and by the corresponding surface equation for CO_2 and CH_4 are shown in Figures 2 to 4, respectively, as a function of pressure and temperature.

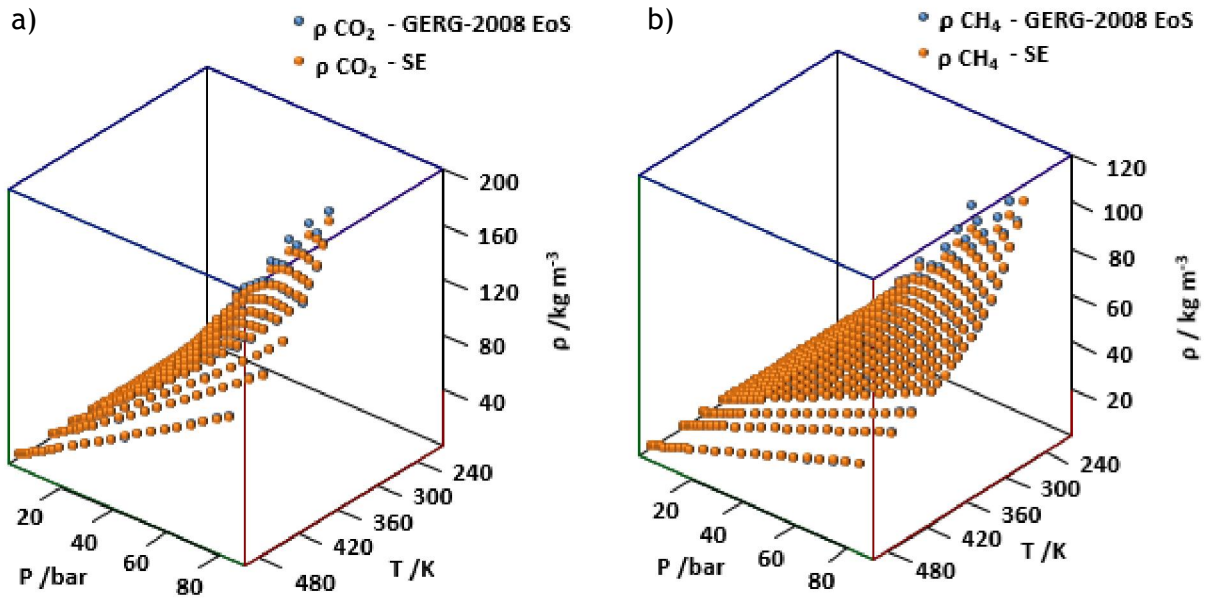

Figure 2 - Density values given by the GERG-2008 EoS and by the corresponding SE as a function of pressure and temperature for: a) pure CO_2; b) pure CH_4.

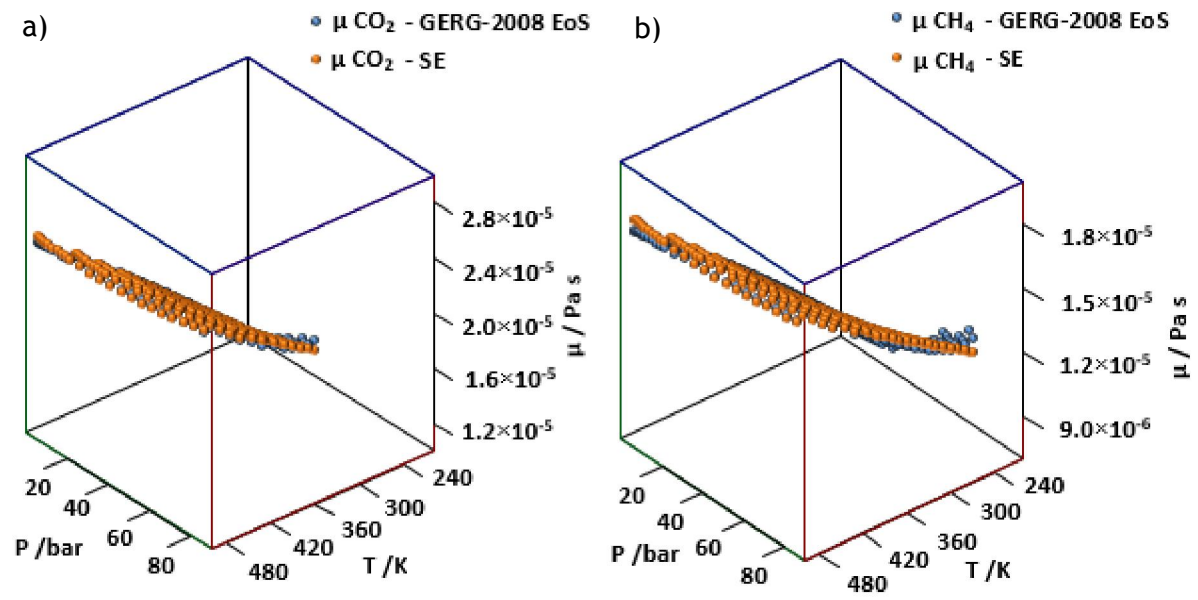

Figure 3 - Viscosity values given by the GERG-2008 EoS and by the corresponding SE as a function of pressure and temperature for: a) pure CO_2; b) pure CH_4.

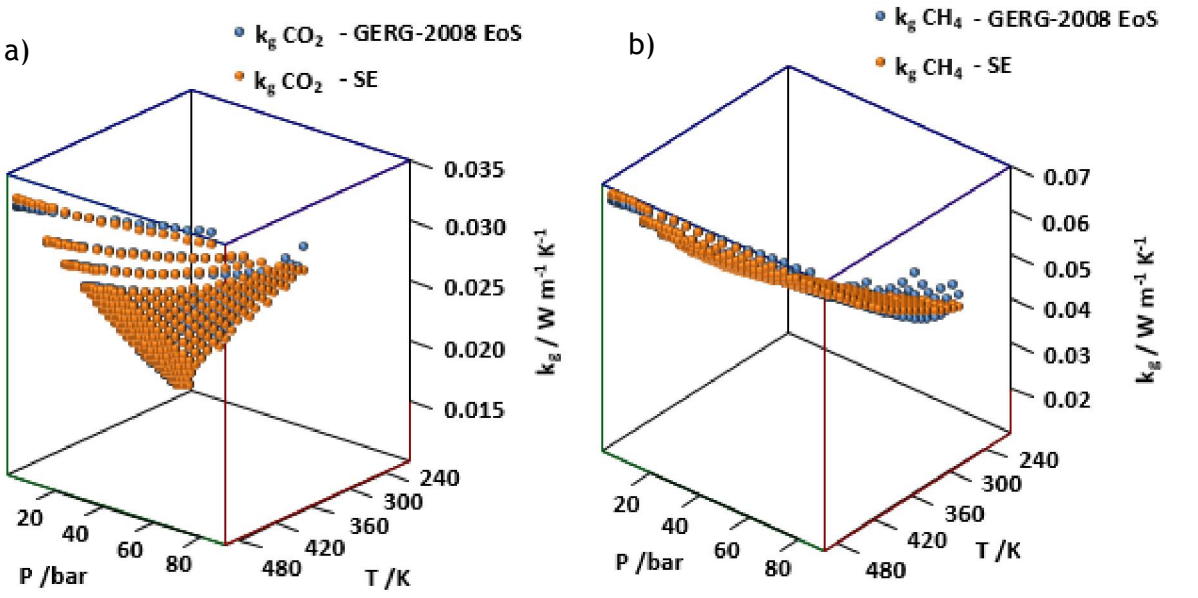

Figure 4 - Thermal conductivity values given by the GERG-2008 EoS and by the corresponding SE as a function of pressure and temperature for: a) pure CO_2; b) pure CH_4.

According to these figures, it is possible to observe that the values determined with the SE are in good agreement with the ones obtained with the GERG-2008 EoS. In fact, the density values calculated with the SE presented a maximum error of 5.6 % at 320 K and 70 bar for CO_2, and 12.6 % at 210 K and 55 bar for CH_4, when compared to the ones obtained with the

reference EoS. A maximum error of 3.9 %, at 330 K and 80 bar, for CO_2 and 7.9 %, at 230 K and 75 bar, for CH_4 were found for the viscosity values. For the thermal conductivity values, it was found a maximum error of 8.3 % for CO_2, at 320 K and 70 bar, and 16 % for CH_4, at 210 K and 55 bar.

For the CO_2/CH_4 mixture, the density, viscosity and thermal conductivity were estimated by the following mixing rules, for mixtures with a molar fraction up to 55 % of CO_2, temperatures from 180 to 480 K and pressures up to 80 bar, considering the SE and respective parameters presented above:

$$\rho = \frac{1}{\sum_{i=1}^{n} \frac{y_{m,i}}{\rho_i}} \tag{34}$$

$$\mu = \sum_{i=1}^{n} y_i \mu_i \tag{35}$$

$$k_g = \sum_{i=1}^{n} y_i k_{g,i} \tag{36}$$

The ρ_i, μ_i, and $k_{g,i}$ represent the SE for density, viscosity, and thermal conductivity for each component of the mixture, respectively, and $y_{m,i}$ is the mass fraction of component *i*.

The compressibility factor and heat capacities at constant pressure and volume SE are presented in Annex A, along with the corresponding parameters.

The values calculated with the SE present a maximum error of 18.7 %, 8.05 %, 15.7 %, 6.6 %, 14.8 % and 11.3 % for the density, viscosity, thermal conductivity, compressibility factor, and heat capacities at constant pressure and volume, respectively, for mixtures with a molar fraction up to 55 % of CO_2.

4.2 Process simulation

In this work, it is intended to replace the cryogenic distillation process reported by Berstad et al. (2012), which was designed to produce a methane stream with a maximum CO_2 content of 50 ppm, with an industrial PTSA process, considering the model detailed in section 3.

According to Berstad et al. (2012), a feed mixture with a molar flow rate of about 6889 mol s^{-1}, containing 50.6 % CO_2, at 313 K and 70 bar, is treated by three sequential columns. The top product of the first column, which presents a CO_2 purity of 10.6 %, is fed to a second column with a flow rate of approximately 3185 mol s^{-1}, at 206 K and 40 bar, to reduce the CO_2 content in CH_4 product further. In the second column, a top product

containing 0.9 % of CO_2, at 185 K and 40 bar, is produced and then fed to a third column. The methane recovery for the second column is around 96.4 %.

In the last column, a methane-rich product with a CO_2 content of 50 ppm is obtained on the top, at 40 bar and 185 K, recovering about 97.5 % of the fed CH_4. The overall recovery of the three columns is about 94 %. Moreira et al. (2017) have successfully replaced this column with a cryogenic PTSA process, where a stream containing 41.8 ppm of CO_2 is produced with a methane recovery of approximately 90.7 %.

4.2.1 Case study 1

The case study 1 corresponds to two parallel and equal PTSA units, designed to replace the entire cryogenic distillation process reported by Berstad et al. (2012). The specifications for each unit of this process are shown in Figure 5. A feed stream of 3444.4 mol s^{-1} with 50.6 % CO_2 at 313 K and 70 bar should be treated to obtain methane with purity above 99.995 %, maximizing its recovery. The adsorbent regeneration is done with part of the methane stream (light product), at 5 bar and 473 K.

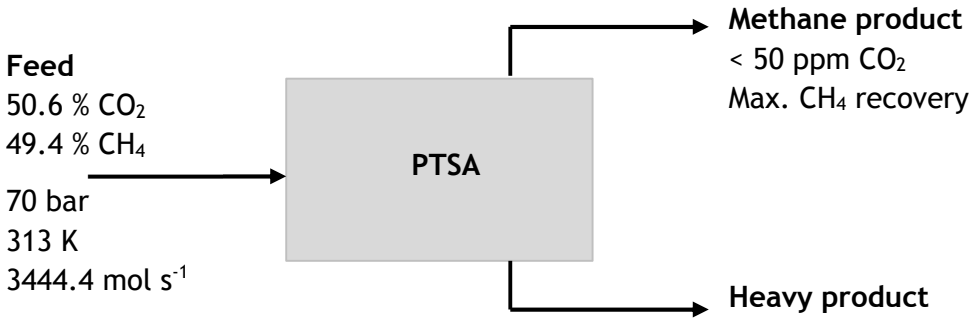

Figure 5 - Block diagram with process specifications for case study 1.

The properties of the binderless zeolite 13X zeolite are shown in Table 6:

Table 6 - Properties of the binderless zeolite 13X adsorbent[a].

Shape	Beads
Particle diameter (mm)	1.6
Particle density (kg m^{-3})	1072
Particle porosity	0.39

[a] Data reported by Moreira et al. (2017).

The parameters of the DSL model for the adsorbent are presented in Table 7:

Table 7 - DSL model parameters for the adsorbent[a].

DSL parameter	CH_4	CO_2
$b_{1,0}$ (bar^{-1})	$2.9x10^{-4}$	$4.1x10^{-4}$
$b_{2,0}$ (bar^{-1})	$1.4x10^{-5}$	$1.3x10^{-5}$
$-\Delta H_1$ (kJ mol^{-1})	15.8	23.0
$-\Delta H_2$ (kJ mol^{-1})	1.9	19.0
$q_{1,0}$ (mmol g^{-1})	3.47	5.78
$q_{2,0}$ (mmol g^{-1})	23.6	1.16
χ_1	0.90	0.51
χ_2	0.002	0.23
T_0 (k)	473	473

[a] Data reported by Moreira et al. (2017).

The characteristics of the bed are presented in Table 8:

Table 8 - Characteristics of the bed for case study 1.

Bed length (m)	10
Internal diameter of the wall (m)	5
Bed porosity	0.4

The fixed bed simulations for the adsorption (co-current pressurization plus feed) and heating steps were run to observe the behavior of the concentration and temperature waves formed inside the column and to determine the required feed time. It was considered that the bed is cooled down during adsorption, instead of using an additional cooling step immediately before, *i.e.*, after the adsorbent regeneration.

Each breakthrough curve was simulated using the OCFEM, with second-order polynomials and 100 intervals, as the numerical method. At the beginning of the adsorption, the column is filled with 50 ppm of CO_2, at 5 bar and 473 K. The feed stream (50.6 % CO_2 + 49.4 % CH_4) is fed to the column until saturation inside the adsorbent particles occurs. In the heating step, an inlet stream containing 50 ppm of CO_2 is fed to the column, which is initially filled with

50.6 % of CO_2 at 313 K and 5 bar. The operating conditions used in the mathematical model are presented in Table 9:

Table 9 - Operating conditions used in the fixed bed simulations for case study 1.

	Adsorption step	Heating step
P (bar)	70	5
T (K)	313	473
F_{in} (mol s^{-1})	3444.4	500
$y_{in,CO2}$	0.506	0.00005 (=50 ppm)

The parameters at feed conditions used in the mathematical model are given in Table 10:

Table 10 - Parameters at feed conditions used in the fixed bed simulations for case study 1.

Parameters	Adsorption step	Heating step
Z	0.7763	0.9928
μ (Pa s)	$1.565x10^{-5}$	$1.663x10^{-5}$
ρ (kg m^{-3})	103.8	2.041
C_p (J mol^{-1} K^{-1})	68.23	45.96
C_v (J mol^{-1} K^{-1})	34.16	36.62
k_g (W m^{-1} K^{-1})	0.03411	0.064316
D_{ax} (m^2 s^{-1})	$1.113x10^{-4}$	$7.7917x10^{-4}$
λ (W m^{-1} K^{-1})	9.747	1.380
k_f (m s^{-1})	$5.704x10^{-3}$	$5.787x10^{-2}$
h_f (W m^{-2} K^{-1})	1075	441
h_w (W m^{-2} K^{-1})	$2.250x10^{4}$	$1.637x10^{3}$

The breakthrough curve (variables' values observed at z = L^-) results relative to the adsorption step are shown in Figure 6, including the behavior of the thermodynamic properties of the mixture obtained with the SE presented in section 4.1.

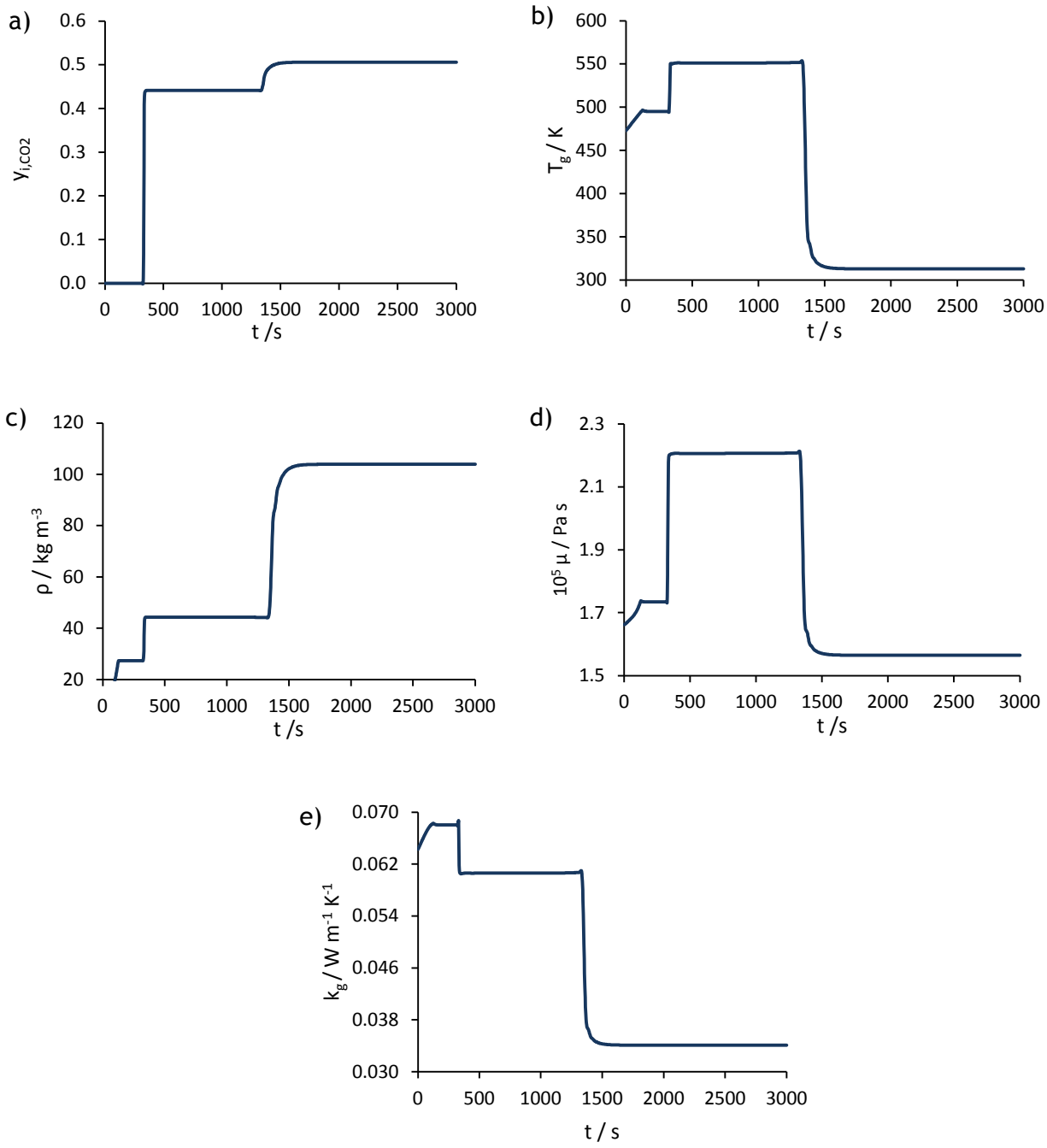

Figure 6 - Breakthrough curve simulation results for the CO_2 adsorption for case study 1: a) CO_2 molar fraction; b) gas temperature; c) density; d) viscosity; e) thermal conductivity at the column outlet.

According to Figure 6 a), the carbon dioxide is completely adsorbed and, consequently, only methane elutes at the column end during the first 330 s, which represents the breakthrough

time. After this, carbon dioxide reaches the top of the column and starts to contaminate the light product. Figure 6 b) shows that the bed temperature rises, since adsorption is an exothermic process, and then decreases due to the cold feed stream. Since the adsorption capacity increases with the decrease of the temperature, it is observed an increase of the CO_2 molar fraction from 0.44 to 0.506 at 1290 s. At the breakthrough time, the mixture density increases and the thermal conductivity decreases, due to the increase of the carbon dioxide concentration at the outlet, despite the influence of the bed temperature.

In Figure 7, the breakthrough curve results for the heating step are presented.

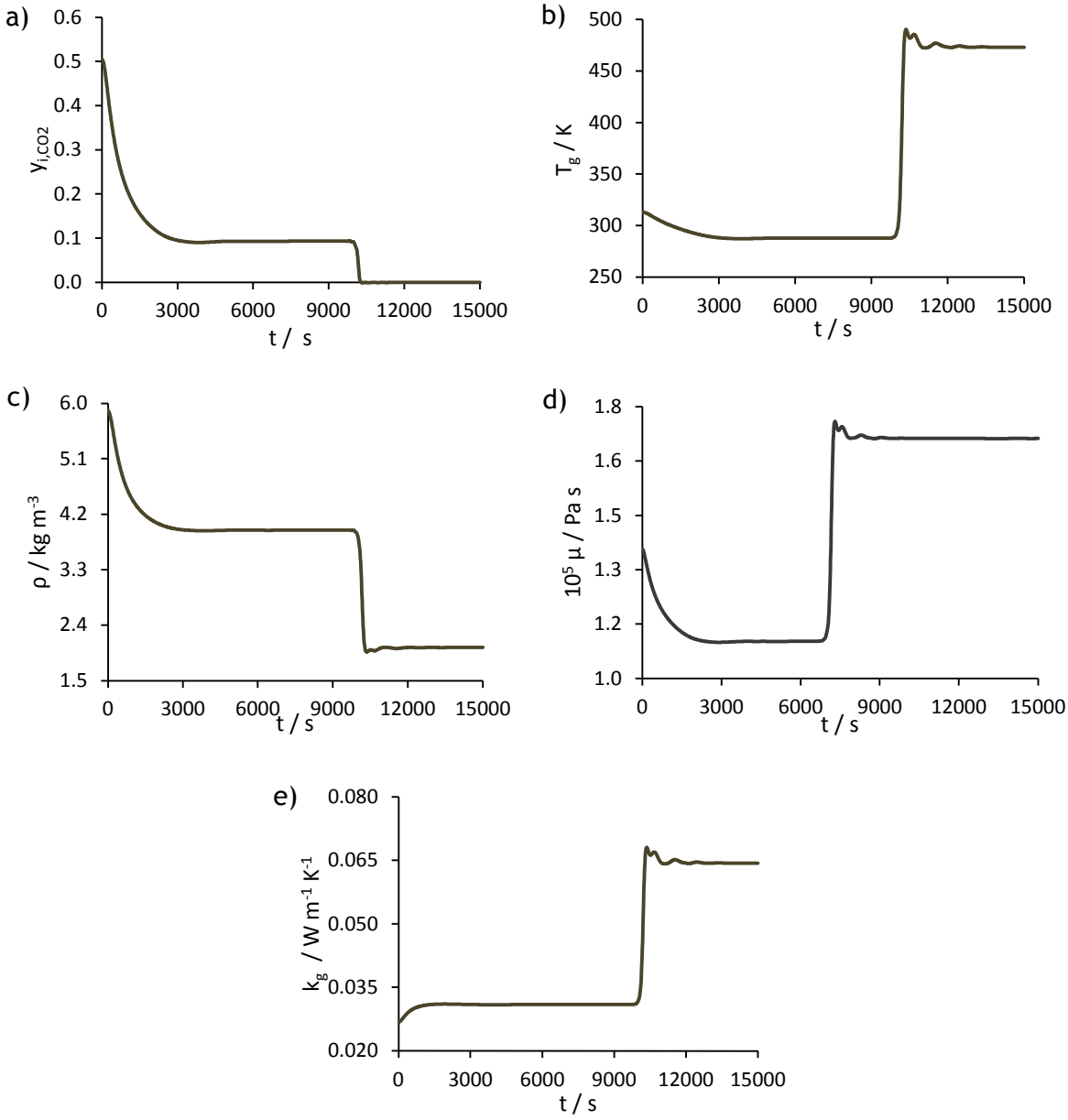

Figure 7 - Breakthrough curve simulation results for the column regeneration for case study 1: a) CO_2 molar fraction; b) gas temperature; c) density; d) viscosity; e) thermal conductivity at the column outlet.

In this figure, it can be observed that the concentration and temperature waves do not behave as expected. At the column outlet, a concentration front of 50.6 % CO_2, at 313 K, should exit first, followed by a higher amount of desorbed CO_2, caused by the increase of the bed temperature, and then by a concentration front of 50 ppm CO_2, at 473 K, that corresponds to the feed conditions.

To further evaluate the behavior of the concentration and temperature waves during the heating step, a slight modification on the case study 1 was made: it was considered that each PTSA unit in parallel was associated in series with another PTSA unit. In this way, instead of reducing the CO_2 concentration from 50.6 % to 50 ppm all at once, the first PTSA in series reduces the CO_2 content from 50.6 % to 10 % or 1 %, and the second one attains the 50 ppm. Fixed bed simulations for the heating step for the first PTSA unit were conducted. The operating conditions for the modified case study 1 are presented in Table 11:

Table 11 - Operating conditions used in the heating step simulation for the modified case study 1.

$y_{in,CO2}$	0.10	0.01
F_{in} (mol s^{-1})	500	500
P (bar)	5	5
T (K)	473	473

The parameters at feed conditions used for the modified case study 1 are given in Table 12:

Table 12 - Parameters at feed conditions used in the heating step simulation for the modified case study 1.

$y_{in,CO2}$	0.10	0.01
Z	0.9940	0.9929
μ (Pa s)	1.728×10^{-5}	1.669×10^{-5}
ρ (kg m^{-3})	2.398	2.076
C_p (J mol^{-1} K^{-1})	45.80	45.94
C_v (J mol^{-1} K^{-1})	36.51	36.61

k_g (W m^{-1} K^{-1})	0.06106	0.06399
D_{ax} (m^2 s^{-1})	$7.801x10^{-4}$	$7.793x10^{-4}$
λ (W m^{-1} K^{-1})	1.356	1.378
k_f (m s^{-1})	0.0596	0.05805
h_f (W m^{-2} K^{-1})	436.2	440.7
h_w (W m^{-2} K^{-1})	1853	1659

The CO_2 molar fraction and temperature histories for the heating step considering the modifications made in the case study 1 are shown in Figure 8:

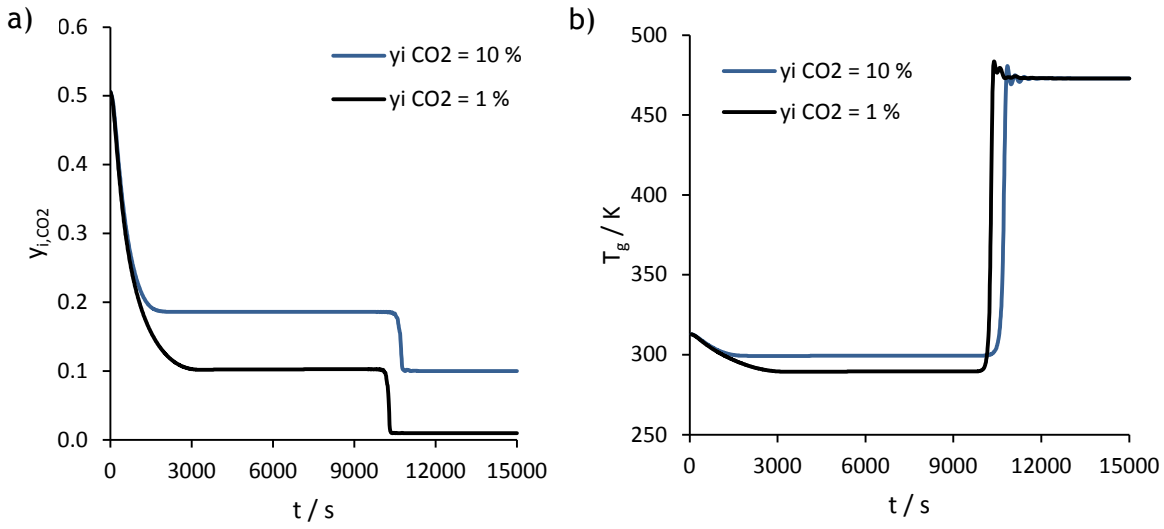

Figure 8 - Breakthrough curve simulation results for the column regeneration for the modified case study 1: a) CO_2 molar fraction; b) gas temperature at the column outlet.

The history of the thermodynamic properties of the mixture determined by the SE developed in the present work are presented in Figure 9 for the modified case study 1:

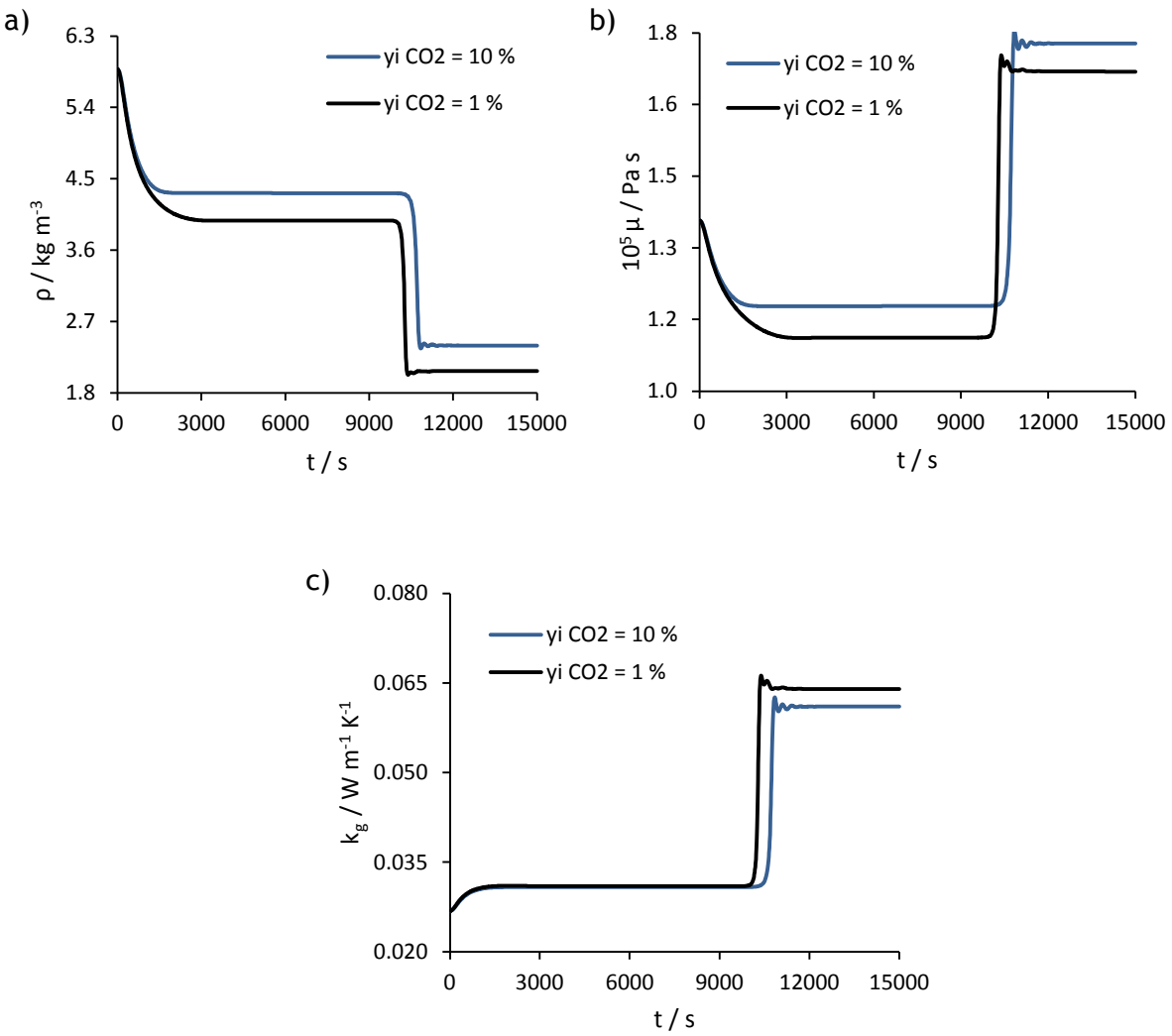

Figure 9 - Breakthrough curve simulation results given by the SE for the column regeneration for the modified case study 1: a) density; b) viscosity; c) thermal conductivity at the column outlet.

As can be seen, the breakthrough curve simulation results considering the carbon dioxide reduction from 50.6 % to 10 % and from 50.6 % to 1 % are similar to the ones presented in Figure 7. Therefore, it can be concluded that the entire replacement of the cryogenic distillation process by PTSA units might not be feasible, and if possible will be hard to achieve.

4.2.2 Case study 2

In case study 2, two parallel and equal PTSA units were designed to replace the last two columns of the distillation process reported by Berstad et al. (2012). The specifications for each PTSA unit of this process are presented in Figure 10. A feed stream of 1593 mol s^{-1} with

10.6 % CO_2 at 206 K e 40 bar should be treated to produce methane with purity above 99.995 %, maximizing its recovery.

The process simulation was done considering that the bed is cooled down during adsorption using the feed stream and that the column regeneration is made with part of the methane stream, at 5 bar and 473 K.

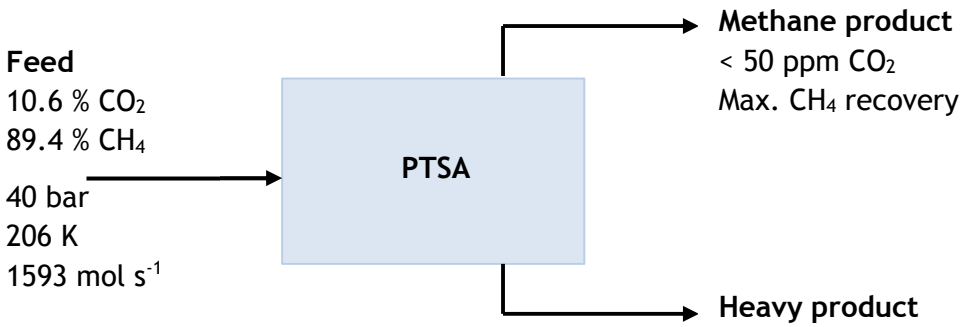

Figure 10 - Block diagram with process specifications for case study 2.

The characteristics of the bed are shown in Table 13:

Table 13 - Characteristics of the bed for case study 2.

Bed length (m)	9
Internal diameter of the wall (m)	5
Bed porosity	0.4

The breakthrough curves for the adsorption (co-current pressurization plus feed) and heating steps were simulated using the OCFEM, with second-order polynomials and 100 intervals, as the numerical method.

In the adsorption step, the natural gas stream (10.6 % CO_2 + 89.4 % CH_4) is fed to the column until saturation is reached, being the column initially filled with 50 ppm of CO_2, at 5 bar and 473 K. An inlet stream containing 50 ppm of CO_2 is fed to the column during the heating step, which is initially filled with 10.6 % of CO_2 at 206 K and 5 bar.

The operating conditions used in the mathematical model are presented in Table 14:

Table 14 - Operating conditions for the fixed bed simulations for case study 2.

	Adsorption step	Heating step
P (bar)	40	5
T (K)	206	473
F_{in} (mol s^{-1})	1593	320
$y_{in,CO2}$	0.106	0.00005 (=50 ppm)

The parameters at feed conditions used in the mathematical model are given in Table 15:

Table 15 - Parameters at feed conditions used in the fixed bed simulations for case study 2.

Parameters	Adsorption step	Heating step
Z	0.6799	0.9928
μ (Pa s)	$9.571x10^{-6}$	$1.663x10^{-5}$
ρ (kg m^{-3})	60.62	2.041
C_p (J mol^{-1} K^{-1})	73.20	45.96
C_v (J mol^{-1} K^{-1})	31.15	36.62
k_g (W m^{-1} K^{-1})	0.02700	0.06432
D_{ax} (m^2 s^{-1})	$5.415x10^{-5}$	$6.360x10^{-4}$
λ (W m^{-1} K^{-1})	4.600	1.045
k_f (m s^{-1})	0.002830	0.0465
h_f (W m^{-2} K^{-1})	584.7	356.3
h_w (W m^{-2} K^{-1})	$1.002x10^4$	$1.048x10^3$

The breakthrough curve results relative to the adsorption step are presented in Figure 11:

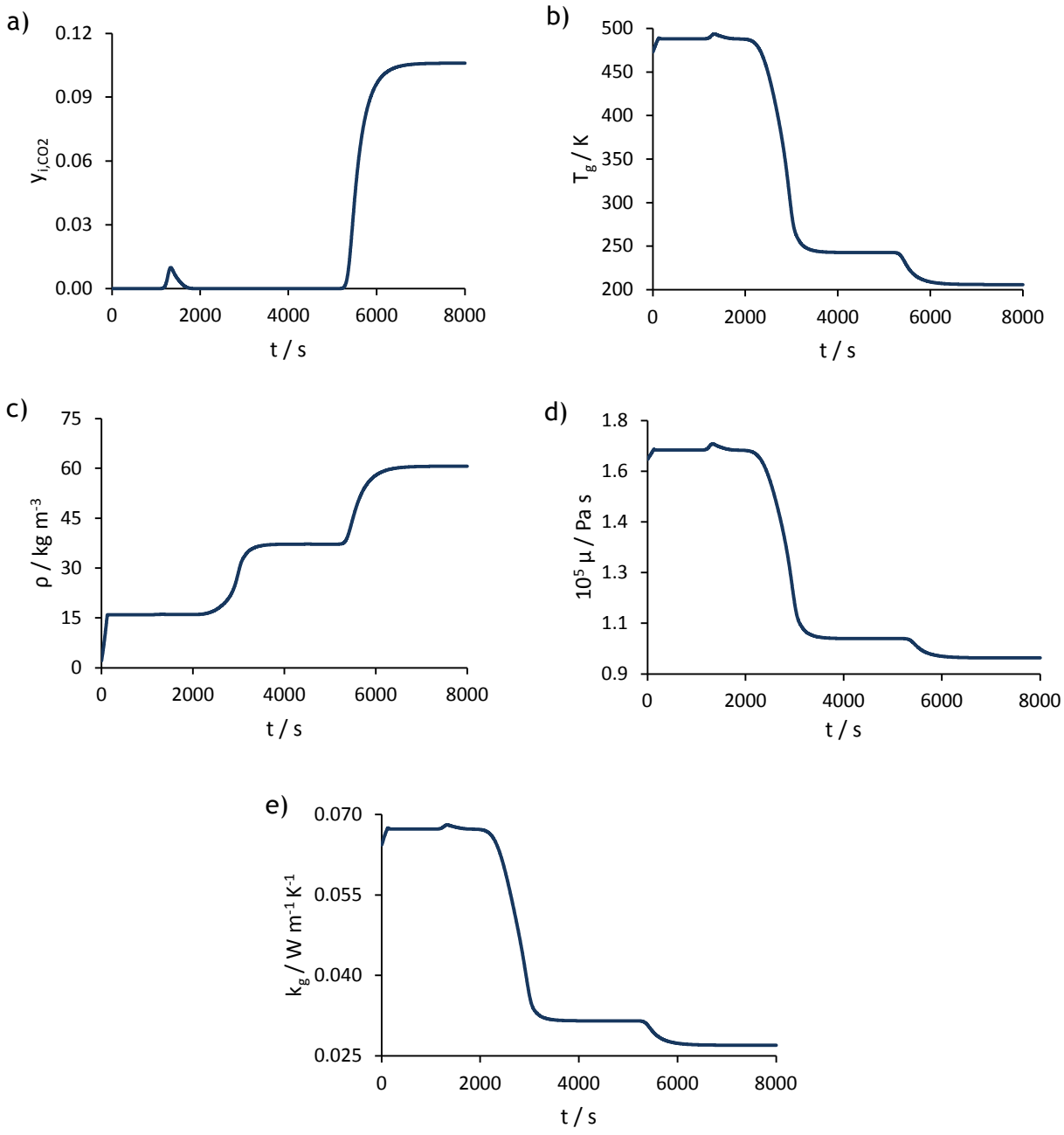

Figure 11 - Breakthrough curve simulation results for the CO_2 adsorption for case study 2: a) CO_2 molar fraction; b) gas temperature; c) density; d) viscosity; e) thermal conductivity at the column outlet.

In Figure 11 a), a peak on the CO_2 molar fraction of about 0.76 % can be observed before the breakthrough time (5300 s), due to a small temperature rise inside the column. The CO_2 adsorption capacity decreases with the increase of the bed temperature, and so a minor amount of carbon dioxide exits the column sooner than expected. According to Figure 11 b), the temperature stabilized at around 242 K before reaching the feed temperature (206 K).

The molar fraction and temperature profiles relative to the adsorption step are presented in Appendix AP.

In Figure 12, the breakthrough curve results for the heating step are presented:

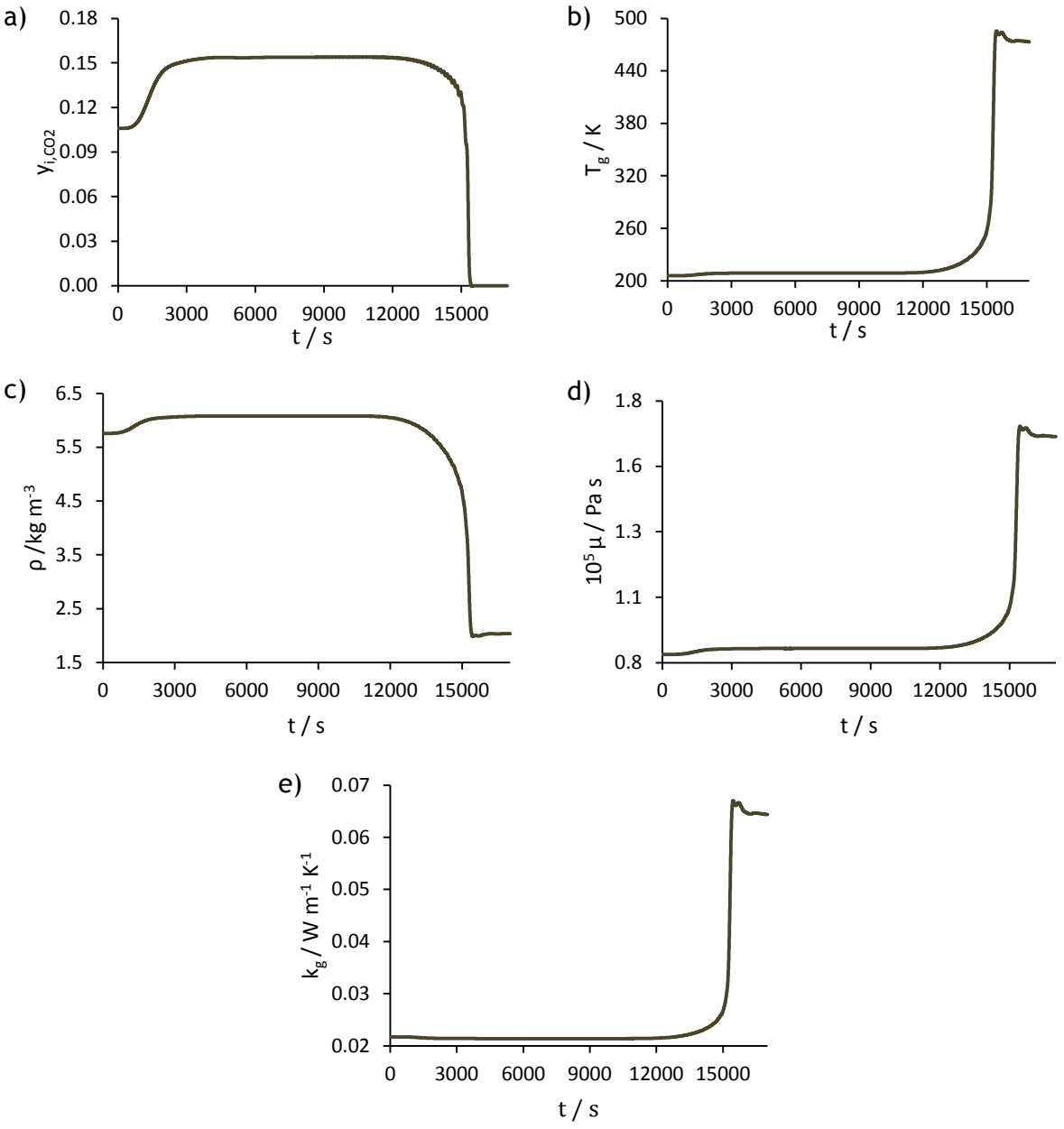

Figure 12 - Breakthrough curve simulation results for the column regeneration for case study 2: a) CO_2 molar fraction; b) gas temperature; c) density; d) viscosity; e) thermal conductivity at the column outlet.

According to Figure 12 a), the CO_2 molar fraction increases from 0.106 to 0.153, due to the slight rise of the bed temperature from 206 to 209 K, and then decreases with the increase of the temperature until the feed conditions are attained. The temperature history shows

that the temperature rises until about 491 K before reaching the inlet temperature (473 K). For both breakthrough curves, the viscosity and thermal conductivity have the same shape of the temperature history, whereas the density presents a behavior identical to the molar fraction instead.

After the breakthrough curve simulation tests, a PTSA cycle was designed and simulated using the OCFEM with second-order polynomials and 60 intervals. Figure 13 presents the proposed PTSA cycle and the corresponding extension for a six-column-unit:

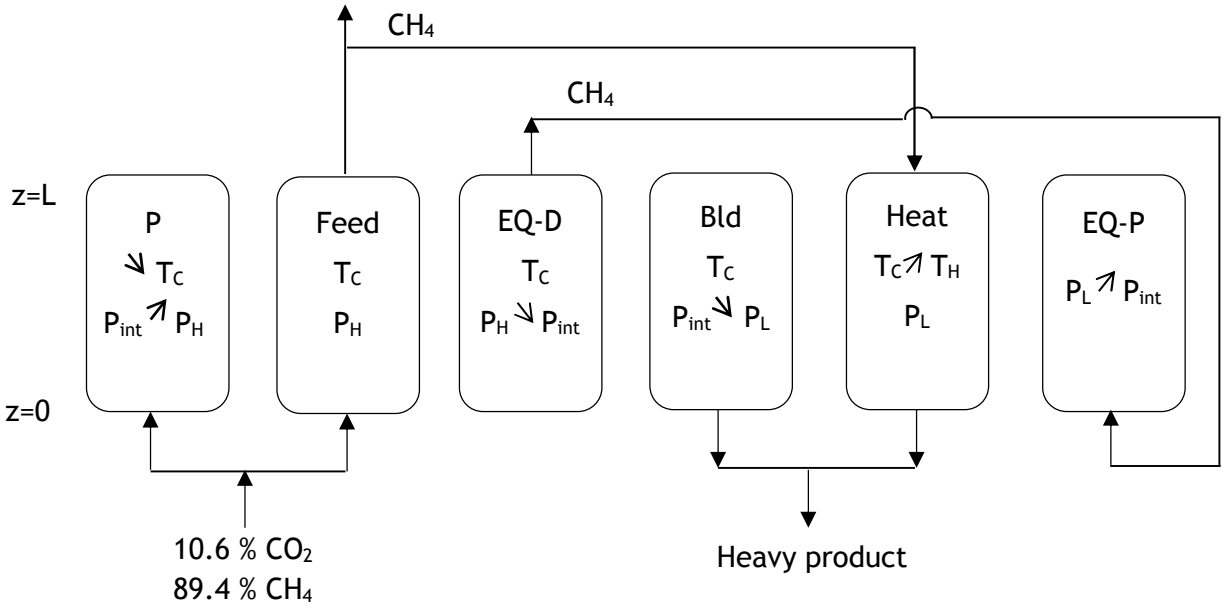

P+Feed	Eq-D	Bld	Heat		Eq-P
Eq-P	P+Feed	Eq-D	Bld	Heat	
Heat	Eq-P	P+Feed	Eq-D	Bld	Heat
Heat		Eq-P	P+Feed	Eq-D	Bld / Heat
Bld	Heat		Eq-P	P+Feed	Eq-D
Eq-D	Bld	Heat		Eq-P	P+Feed

Figure 13 - Proposed PTSA cycle for case study 2.

The PTSA cycle is composed of the following six steps:

- Co-current pressurization and feed -adsorption-, where a stream rich in methane is fed to the column at a low temperature (T_C), producing a light product at high pressure (P_H);
- Co-current pressure equalization-depressurization until an intermediate pressure (P_{int}) is achieved;
- Counter-current blowdown until low pressure (P_L) is attained;
- Heating, where the light product is fed counter-currently at a high temperature (T_H), producing a heavy product at the outlet of the column;
- Co-current pressure equalization-pressurization until the intermediate pressure is once again achieved.

For the extension to a six-column unit, the duration of each pressure equalization step was set to be equal to the pressurization plus feed steps. The duration of the blowdown plus heating step was considered to be three times the pressurization plus feed steps. In this way, an adsorption step time of 5300 s and a blowdown step of 600 s were defined. Thus, the total cycle time is 31800 s (8.8 h).

The operating conditions used in the mathematical model are presented in Table 16:

Table 16 - Operating conditions used in the PTSA cycle simulations for case study 2.

T_C (K)	206
T_H (K)	473
P_H (bar)	40
P_L (bar)	5
P_{int} (bar)	24.2
$y_{in,feed}$	0.106
F_{in} (mol s^{-1})	Feed:1593; EQ-P:20.4; Heat:320
Step times (s)	P+Feed:5300; EQ-D:5300; Bld:600; Heat:15300; EQ-P:5300

The CO_2 molar fraction, pressure, and temperature values obtained at the column outlet during one cycle in CSS are shown in Figure 14:

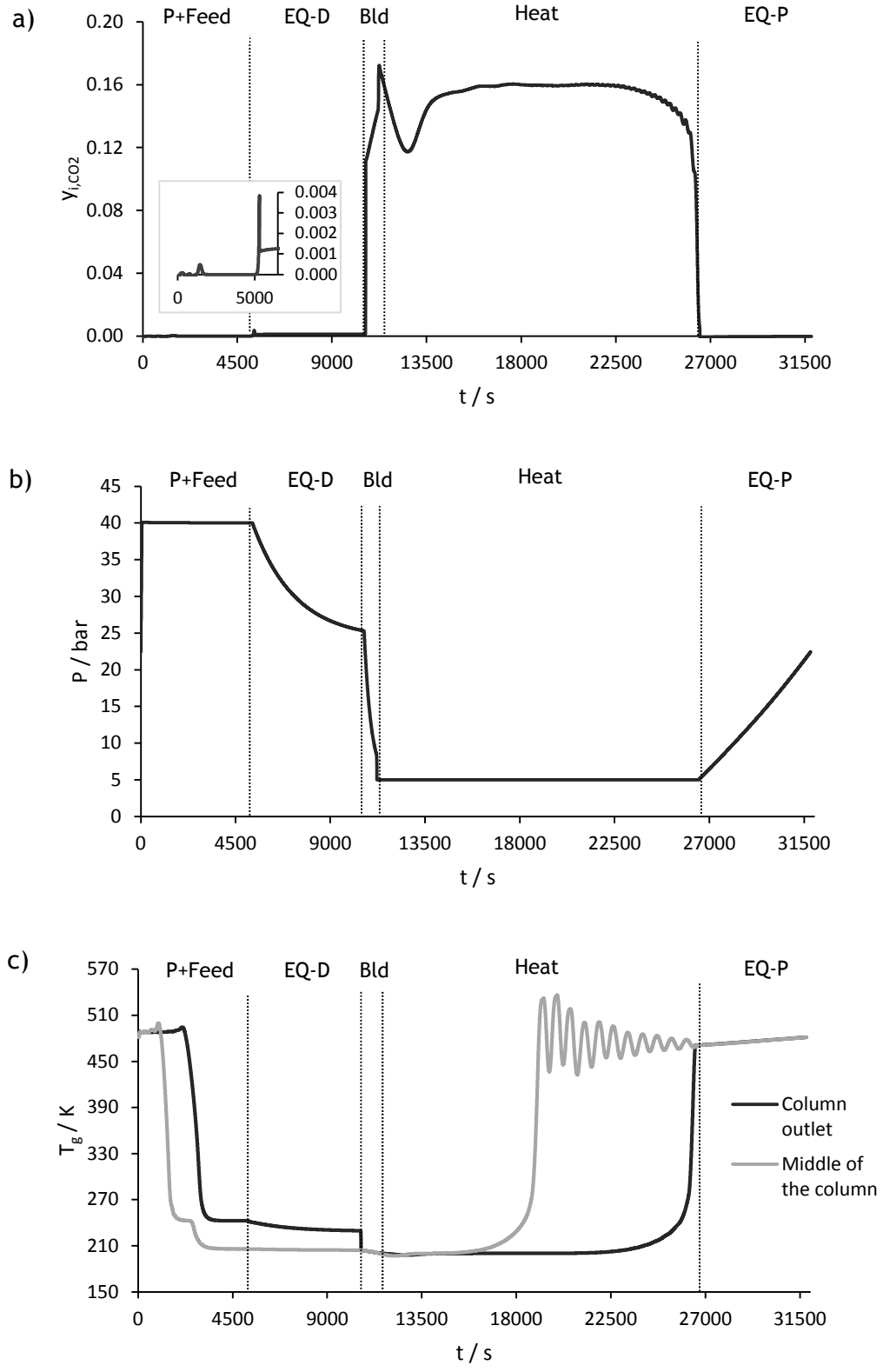

Figure 14 - PTSA cycle simulation results at CSS for case study 2: a) CO_2 molar fraction at the column outlet; b) pressure at the column outlet; c) gas temperature at the outlet and middle of the column.

This figure shows that practically all carbon dioxide is adsorbed during the pressurization plus feed time, resulting in the production of a methane stream with high purity (< 50 ppm CO_2). A peak in the carbon dioxide molar fraction (around 0.047 %) can be seen at 1470 s, caused by a sudden rise in the gas temperature, which may affect the performance of the system. In the pressure history, it can be observed that the pressurization happens very rapidly prior to the adsorption step.

In the pressure equalization-depressurization step, the pressure is reduced from 40 to 24.2 bar, which results in the slight desorption of carbon dioxide and, consequently, in the decrease in the bed temperature. The pressure is further reduced to 5 bar during the blowdown step, and the adsorbent is regenerated, since carbon dioxide desorbs and exits the column. It can be observed a decrease in the gas temperature in the blowdown step, due to the fact that desorption is an endothermic phenomenon.

During the heating step, the column continues to be regenerated. The increase of the gas temperature allows a significant amount of CO_2 to exit the column. In the pressure equalization-pressurization step, the pressure increases until 24.2 bar, and the gas temperature slightly increases, which can be related to the carbon dioxide adsorption.

The performance parameters obtained in the cyclic simulation are presented in Table 17:

Table 17 – Performance evaluation of the proposed PTSA cycle for case study 2.

	Methane product	Heavy product
Purity (%)	99.9954 (46 ppm CO_2)	15.1
Recovery (%)	33.16	99.98
Productivity (mol^{-1} kg^{-1} h^{-1})	2.49	-
Power consumption (MW)		3.6

According to Table 17, it is possible to obtain a methane product with a purity higher than 99.995 % using the proposed PTSA cycle, but with a low methane recovery, which is approximately 33.16 %. Thus, the methane recovery obtained in this process is much lower when compared to the one associated with the cryogenic distillation process. It can also be concluded that the power consumption of the proposed process is relatively low.

The influence of the adsorption step time and inlet flow rate used in the heating step on the PTSA performance (methane purity and recovery) were assessed. The results obtained are presented in Figure 15:

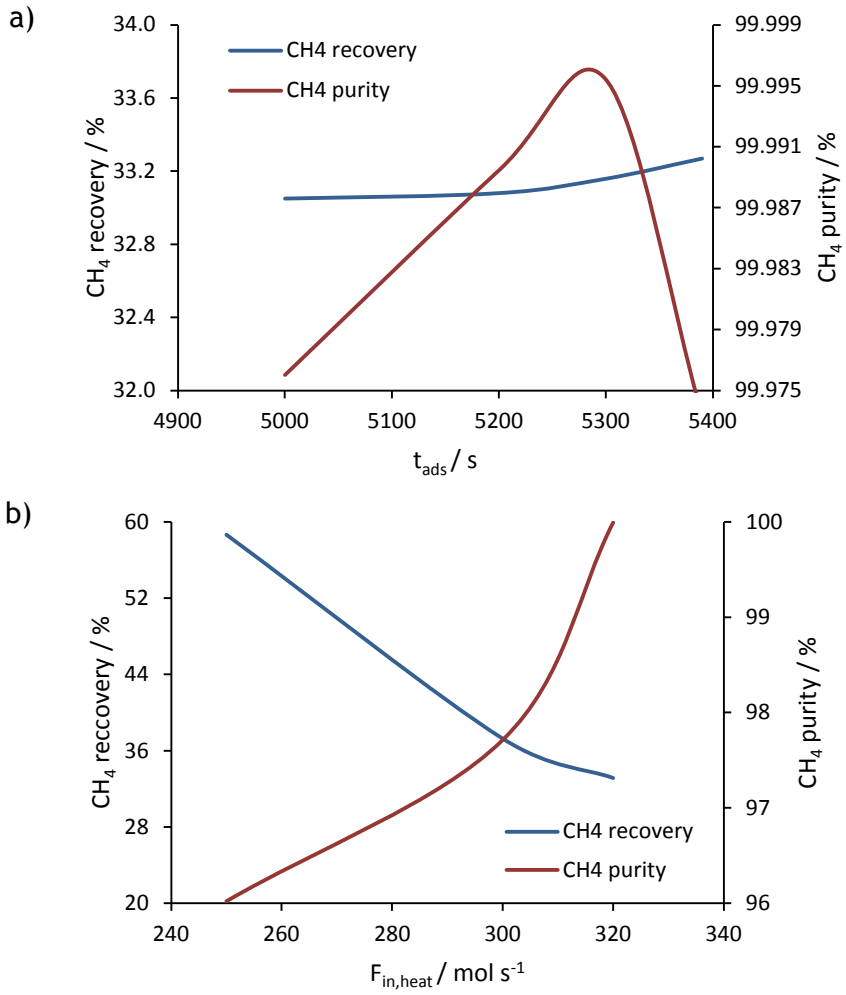

Figure 15 - Influence of the operating conditions on the PTSA performance: a) effect of the adsorption step time; b) effect of the inlet flow rate used in the heating step.

According to this figure, the methane purity increases with the adsorption step time until about 5300 s and then decreases. The increase of the methane purity with the adsorption step time may be caused by the spike on the carbon dioxide concentration that happens during adsorption (see Figure 14), and so its influence may be more significant when the adsorption time is too short. On the other hand, methane recovery increases when the adsorption step time increases.

It can also be observed that methane purity increases when the inlet flow rate used in the heating step is increased, while the methane recovery decreases.

4.2.3 Case study 3

A different PTSA cycle was designed and simulated using the OCFEM with second-order polynomials and 50 intervals, considering the process specifications presented in case study 2. Figure 16 shows the proposed PTSA cycle and the corresponding extension for a four-column-unit:

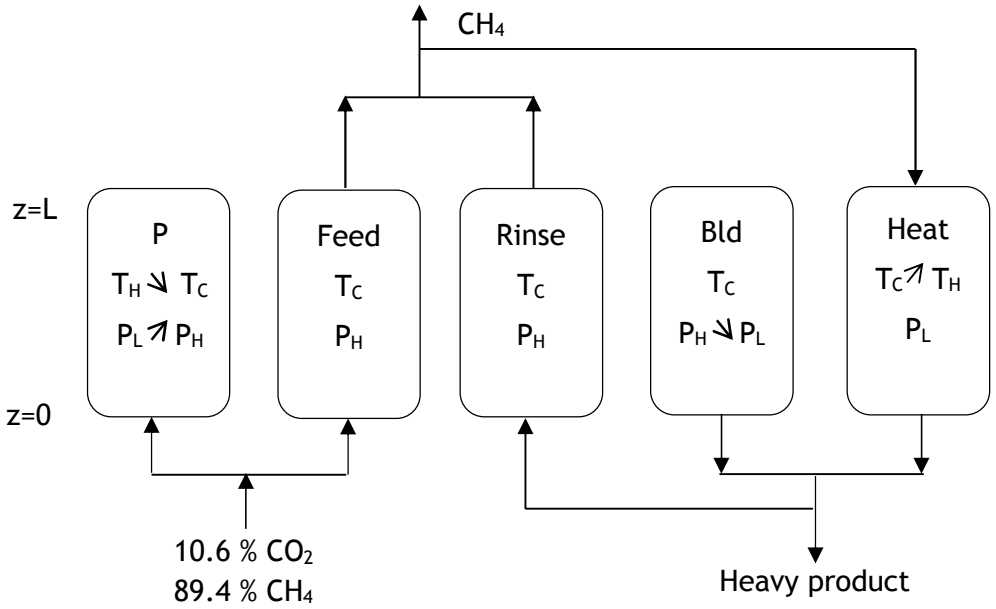

P+Feed			Rinse			Bld	Heat	Heat	
Heat			P+Feed			Rinse		Bld	Heat
Bld	Heat		Heat			P+Feed		Rinse	
Rinse			Bld	Heat		Heat		P+Feed	

Figure 16 – Proposed PTSA cycle for case study 3.

The PTSA cycle is composed of the following five steps: co-current pressurization and feed (adsorption); rinse, where the heavy product passes through the column co-currently; counter-current blowdown; and heating. For the extension to a four-column unit, the duration of the rinse step was set to be equal to the pressurization plus feed step. The duration of the blowdown plus heating step was considered to be two times the pressurization plus feed step. An adsorption step time of 5300 s and a blowdown step of 250 s were defined. Therefore, the total cycle time is 21200 s, which corresponds to about 5.9 h.

The operating conditions used in the mathematical model are presented in Table 18:

Table 18 - Operating conditions used in the PTSA cycle simulations for case study 3.

T_C (K)	206
T_H (K)	473
P_H (bar)	40
P_L (bar)	5
$y_{in,feed}$	0.106
F_{in} (mol s^{-1})	Feed:1593; Rinse:75; Heat:500
Step times (s)	P+Feed:5300; Rinse:5300; Bld:250; Heat:10350

The CO_2 molar fraction and temperature values obtained at the column outlet during one cycle in CSS are shown in Figure 17:

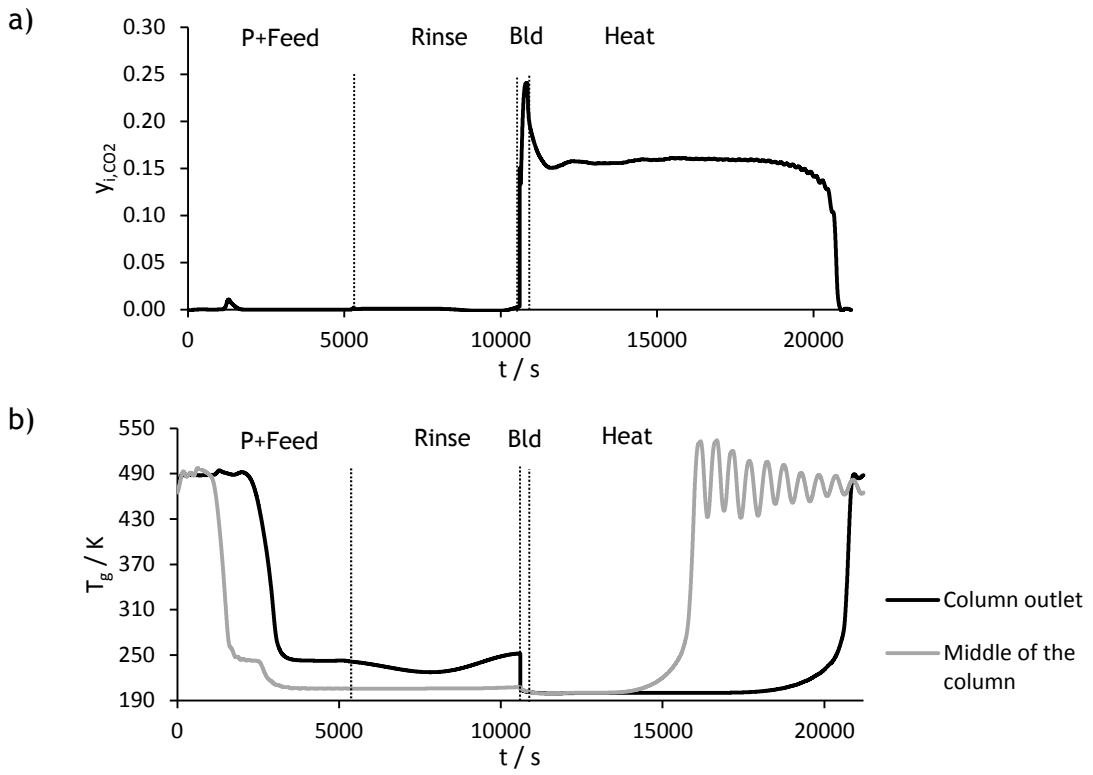

Figure 17 - PTSA cycle simulation results at CSS for case study 3: a) CO_2 molar fraction at the column outlet; b) gas temperature at the outlet and middle of the column.

In this figure, a peak in the carbon dioxide molar fraction (around 0.88 %) can once again be observed during the adsorption step. According to the temperature history, the gas temperature increases during the rinse step, since adsorption is occurring inside the column.

The extension to a two-column unit was not done in this work, since it required a high molar flow rate and, consequently, a high velocity in the heating step (about 0.45 m s^{-1}) to equalize the adsorption plus rinse steps with the blowdown plus heating steps.

The performance parameters obtained in the cyclic simulation are presented in Table 19:

Table 19 - Performance evaluation of the proposed PTSA cycle for case study 3.

	Methane product	Heavy product
Purity (%)	99.95	15.0
Recovery (%)	32.98	99.86
Productivity (mol^{-1} kg^{-1} h^{-1})	3.72	-
Power consumption (MW)		6.1

Although the proposed PTSA cycle allows the production of a relatively pure methane product, it is possible to see that it does not satisfy the specifications for the LNG transport (> 99.995 %). The methane recovery obtained is slightly inferior to the one determined in case study 2, with the pressure equalization steps, and the power consumption is higher.

Therefore, the addition of pressure equalization steps leads to better results than adding the rinse step. To improve the methane recovery, the pressure equalization steps and the rinse step may be used together. Besides, a cooling step, where a cooling fluid passes through the column before the adsorption step, may be added to the process.

5 Conclusion

In this work, a pressure temperature swing adsorption process was designed and optimized to produce a methane product with a purity inferior to 99.995 % for the liquified natural gas transport. The possibility of replacing an existing multicolumn cryogenic distillation process was evaluated. The modeling of the dynamic behavior of the process was done, considering that surface equations represent well the thermodynamic properties of the mixture. The surface equations were developed by adjusting the values given by the REFPROP software package with the GERG-2008 as the equation of state to reduce the computational time.

It was possible to conclude that the values obtained with the SE present a maximum error of 18.7 %, 8.05 %, 15.7 %, 6.6 %, 14.8 % and 11.3 % for the density, viscosity, thermal conductivity, compressibility factor, and heat capacities at constant pressure and volume, respectively, for mixtures with a molar fraction up to 55 % of CO_2.

The simulation results showed that the entire replacement of the cryogenic distillation process, which allows the reduction of a carbon dioxide concentration from 50.6 % to 50 ppm, by a PTSA process is not feasible. However, the last two columns of the distillation process can be replaced by a PTSA technology that can reduce the carbon dioxide content from 10.6 % to 46 ppm, with a methane recovery of about 33.16 % and power consumption of 3.6 MW, for the case where pressure equalization steps were added to the system. It was also achieved a methane productivity of 2.49 mol^{-1} kg^{-1} h^{-1}. The PTSA cycle presents a lower methane recovery when compared to the distillation process (33.16 % against 96.4 %).

The influence of the adsorption step time and inlet flow rate used in the heating step on the performance of the PTSA composed by pressure equalization steps was assessed. The methane purity firstly increases with the adsorption step duration. It then decreases, which can be explained by the occurrence of a spike on the carbon dioxide concentration that happens during adsorption, which is caused by a rise in the gas temperature. The methane recovery increases when the adsorption step time is increased. The increase of the inlet flow rate used in the heating step leads to the rise in the methane purity and a drop on its recovery.

Considering the PTSA process with the rinse step, it is possible to conclude that it does not produce a methane product with the required specifications for the liquified natural gas transport (> 99.995 %). The methane recovery obtained is slightly inferior to the one determined in the case with the pressure equalization steps, and the power consumption is higher (32.98 % and 6.1 MW, respectively). It was also achieved a methane productivity of 3.72 mol^{-1} kg^{-1} h^{-1}.

For future work, other steps may be added to the PTSA cycle to improve the performance of the system, especially the methane recovery. A rinse step and/or a cooling step, where a cooling fluid goes through the column before the adsorption step, could be added to the PTSA cycle containing already pressure equalization steps. The reason why a cooling step is being considered has to do with the sudden rise in the temperature before the adsorption time is interrupted that causes the exit of a small amount of carbon dioxide. If the decrease in the gas temperature is performed before the pressurization plus feed steps, then this spike in the carbon dioxide concentration disappears, which may increase the system performance.

Other option is to consider another adsorbent, which might be less sensitive to CO_2 adsorption, *i.e.*, with a lower heat of adsorption for CO_2. A potential candidate is the MOF UiO-66(Zr)_$(COOH)_2$ which has been already screened for this application. Another study that must be done is to further verify the feasibility of reducing the CO_2 content from 50.6 % to 10.6 % with advanced PTSA processes.

6 Assessment of the work done

6.1 Objectives achieved

One of the objectives of this thesis was to developed surface equations that would represent the behavior of the thermodynamic properties. Considering the maximum errors that were determined, it can be concluded that the surface equations, in fact, are an excellent choice to reduce the computational time of the simulations while leading to accurate information.

The main goal of this thesis was to simulate and design an industrial scale pressure temperature swing adsorption process to produce a methane product with the requirements for the liquified natural gas transport that could replace a cryogenic distillation process composed by three sequential columns. It can be concluded that the entire replacement of this process was not feasible. However, the replacement of the last two columns can be done using a PTSA cycle that includes pressure equalization steps. This PTSA cycle results in the production of a methane product with a carbon dioxide content inferior to 50 ppm, but with a low methane recovery. Thus, ways to increase the performance of the system should be pursued.

6.2 Final assessment

The present work is a solid starting point for the development of an advance pressure temperature swing adsorption cycle that could allow the complete replacement of the cryogenic distillation plant with high efficiency.

7 References

Berstad, D., Neksa, P., & Anantharaman, R. (2012). Low-temperature CO2 removal from natural gas. *2nd Trondheim Gas Technology Conference, 26*, 41-48. doi:10.1016/j.egypro.2012.06.008

Bird, R. B., W. E Stewart, and E. N Lightfoot. (2002). *Transport Phenomena*. New York, NY.: Wiley.

Campo, M. C., Ribeiro, A. M., Ferreira, A. F. P., Santos, J. C., Lutz, C., Loureiro, J. M., & Rodrigues, A. E. (2016). Carbon dioxide removal for methane upgrade by a VSA process using an improved 13X zeolite. *Fuel Processing Technology, 143*, 185-194. doi:10.1016/j.fuproc.2015.11.024

Carmo, P., Ribeiro, A., Rodrigues, A., & Ferreira, A. (2018). Modeling and Simulation of a TPSA System for a Vinyl Chloride/Nitrogen Separation from Industrial Streams. *Industrial & Engineering Chemistry Research, 57(42), 14223-14232. doi: 10.1021/acs.iec*.

Da Silva, F. A. (1999). Cyclic Adsorption Processes: Application To Propane/Propylene Separation. In. Ph.D. Dissertation, University of Porto.

Da Silva, F. A., Silva, J. A., & Rodrigues, A. E. (1999). A general package for the simulation of cyclic adsorption processes. *Adsorption-Journal of the International Adsorption Society, 5*(3), 229-244.

Dauber, F., & Span, R. (2012). Modelling liquefied-natural-gas processes using highly accurate property models. *Applied Energy, 97*, 822-827.

Do, D. D. (1998). *Adsorption analysis: equilibria and kinetics* (Vol. 2): Imperial college press London.

Ferreira, A. F. P., Ribeiro, A. M., Kulac, S., & Rodrigues, A. E. (2015). Methane purification by adsorptive processes on MIL-53(Al). *Chemical Engineering Science, 124*, 79-95. doi:10.1016/j.ces.2014.06.014

Kamakoti, P., Leta, D.P., Deckman, H.W., Ravikovitch, P.I, Anderson, T.N. (2014). US Patent No. 8,784,534 B2.

Kunz, O., & Wagner, W. (2012). The GERG-2008 wide-range equation of state for natural gases and other mixtures: an expansion of GERG-2004. *Journal of chemical & engineering data, 57*(11), 3032-3091.

Malik, R. L. (1994). US Patent No. 5,298,054.

Mokhatab, S., Poe, W. A., & Mak, J. (2019). *Handbook of natural gas transmission and processing : principles and practices*.

Moreira, M. A., Ribeiro, A. M., Ferreira, A. P. P., & Rodrigues, A. E. (2017). Cryogenic pressure temperature swing adsorption process for natural gas upgrade. *Separation and Purification Technology, 173*, 339-356. doi:10.1016/j.seppur.2016.09.044

Pour, A. A., Sharifnia, S., NeishaboriSalehi, R., & Ghodrati, M. (2015). Performance evaluation of clinoptilolite and 13X zeolites in CO2 separation from CO2/CH4 mixture. *Journal of Natural Gas Science and Engineering, 26*, 1246-1253.

PSE: Products - Gproms - Custom Modelling. (2020, Jun 1). *Psenterprise.Com*. Retrieved from https://www.psenterprise.com/products/gproms/custom

Qiu, L. Y., Murashov, V., & White, M. A. (2000). Zeolite 4A: heat capacity and thermodynamic properties. *Solid State Sciences, 2*(8), 841-846. doi:Doi 10.1016/S1293-2558(00)01102-X

Ravikovitch, P. I., Johnson, R.A., Deckman, H.W., Anderson, T.N. (2014). US Patent No. 8,784,535 B2.

Ribeiro, A. M., Grande, C. A., Lopes, F. V., Loureiro, J. M., & Rodrigues, A. E. (2008). A parametric study of layered bed PSA for hydrogen purification. *Chemical Engineering Science, 63*(21), 5258-5273.

Rowland, D., Hughes, T. J., & May, E. F. (2016). Extending the GERG-2008 equation of state: Improved departure function and interaction parameters for (methane+ butane). *The Journal of Chemical Thermodynamics, 97*, 206-213.

Ruthven, D. M. (1984). *Principles of adsorption and adsorption processes*: John Wiley & Sons.

Shimekit, B., & Mukhtar, H. (2012). Natural gas purification technologies-major advances for CO2 separation and future directions. *Advances in natural gas technology, 9*, 235-270.

Speight, J. G. (2018). *Handbook of Natural Gas Analysis*: Wiley Online Library.

Varzandeh, F., Stenby, E. H., & Yan, W. (2017). Comparison of GERG-2008 and simpler EoS models in calculation of phase equilibrium and physical properties of natural gas related systems. Fluid Phase Equilibria, 434, 21-43.

Vikse, M., Watson, H. A. J., Gundersen, T., & Barton, P. I. (2018). Simulation of Dual Mixed Refrigerant Natural Gas Liquefaction Processes Using a Nonsmooth Framework. *Processes, 6*(10). doi:ARTN 19310.3390/pr6100193

Viswanathan, B. (2016). *Energy sources: fundamentals of chemical conversion processes and applications*: Newnes.

Yang, R. T. (1987). *Gas Separation by Adsorption Processes*: Butterworth-Heinemann.

Zhao, R., Zhao, L., Deng, S., Song, C., He, J., Shao, Y., & Li, S. (2017). A comparative study on CO2 capture performance of vacuum-pressure swing adsorption and pressure-temperature swing adsorption based on carbon pump cycle. *Energy, 137*, 495-509.

Zhao, R. K., Liu, L. C., Zhao, L., Deng, S., Li, S. J., Zhang, Y., & Li, H. L. (2019). Techno-economic analysis of carbon capture from a coal-fired power plant integrating solar-assisted pressure-temperature swing adsorption (PTSA). *Journal of Cleaner Production, 214*, 440-451. doi:10.1016/j.jclepro.2018.12.316

Zhao, R. K., Zhao, L., Wang, S. P., Deng, S., Li, H. L., & Yu, Z. X. (2018). Solar-assisted pressure-temperature swing adsorption for CO2 capture: Effect of adsorbent materials. *Solar Energy Materials and Solar Cells, 185*, 494-504. doi:10.1016/j.solmat.2018.06.004

Annex A - Surface equations

The surface equations of the compressibility factor and heat capacities at constant volume and pressure for pure CH_4 and pure CO_2, valid for a temperature range between 180 and 480 K and pressures from 0.1 to 80 bar, are presented in Table A.1 (Moreira et al., 2017):

Table A.1 - Compressibility factor and heat capacities at constant volume and pressure surface equations.

$Z_i = a + \frac{b}{T_g} + cP + d\frac{P}{T_g} + e\frac{P}{{T_g}^2}$
$C_{p,i} = a + bT_g + cP + d{T_g}^2 + eT_gP + fP^2 + g{T_g}^3 + h{T_g}^2P + jT_gP^2 + kP^3 + l{T_g}^4 + m{T_g}^3P + n{T_g}^2P^2 + oT_gP^3$
$C_{v,i} = a + bT_g + cP + d{T_g}^2 + eT_gP + fP^2 + g{T_g}^3 + h{T_g}^2P + jT_gP^2 + kP^3 + l{T_g}^4 + m{T_g}^3P + n{T_g}^2P^2 + oT_gP^3$

Table A.2 shows the respective SE parameters (adapted from Moreira et al. (2017)):

Table A.2 - Parameters of the surface equations for the compressibility factor and heat capacities at constant volume and pressure.

Thermodynamic property	SE Parameter	CH_4	CO_2
Compressibility factor	a	-7.21×10^{-5}	-7.64×10^{-4}
	b (K)	0.030	0.25
	c (Pa^{-1})	-5.65×10^{-8}	2.82×10^{-8}
	d (K Pa^{-1})	4.57×10^{-5}	7.26×10^{-6}
	f (K^2 Pa^{-1})	-0.010	-0.010
Heat capacity at constant pressure	a (J mol^{-1} K^{-1})	247.7	157.9
	b (J mol^{-1} K^{-2})	-3.044	-1.823
	c (J mol^{-1} K^{-1} Pa^{-1})	8.53×10^{-5}	2.32×10^{-4}
	d (J mol^{-1} K^{-3})	0.0154	0.00931

	e (J mol^{-1} K^{-2} Pa^{-1})	$-7.73x10^{-7}$	$-1.92x10^{-6}$
	f (J mol^{-1} K^{-1} Pa^{-2})	$4.10x10^{-12}$	$1.82x10^{-11}$
	g (J mol^{-1} K^{-4})	$-3.32x10^{-5}$	$-1.98x10^{-5}$
	h (J mol^{-1} K^{-3} Pa^{-1})	$2.23x10^{-9}$	$5.22x10^{-9}$
	j (J mol^{-1} K^{-2} Pa^{-2})	$-1.53x10^{-14}$	$-8.68x10^{-14}$
	k (J mol^{-1} K^{-1} Pa^{-3})	$-2.02x10^{-19}$	$-1.08x10^{-20}$
	l (J mol^{-1} K^{-5})	$2.58x10^{-8}$	$1.51x10^{-8}$
	m (J mol^{-1} K^{-4} Pa^{-1})	$-2.05x10^{-12}$	$-4.64x10^{-12}$
	n (J mol^{-1} K^{-3} Pa^{-2})	$1.06x10^{-17}$	$1.01x10^{-16}$
	o (J mol^{-1} K^{-2} Pa^{-3})	$5.69x10^{-22}$	$7.60x10^{-23}$
Heat capacity at constant volume	a (J mol^{-1} K^{-1})	50.58	40.7
	b (J mol^{-1} K^{-2})	-0.337	-0.302
	c (J mol^{-1} K^{-1} Pa^{-1})	$8.97x10^{-6}$	$4.90x10^{-5}$
	d (J mol^{-1} K^{-3})	0.00152	0.00168
	e (J mol^{-1} K^{-2} Pa^{-1})	$-7.21x10^{-8}$	$-3.66x10^{-7}$
	f (J mol^{-1} K^{-1} Pa^{-2})	$2.83x10^{-14}$	$1.38x10^{-12}$
	g (J mol^{-1} K^{-4})	$-2.77x10^{-6}$	$-3.43x10^{-6}$
	h (J mol^{-1} K^{-3} Pa^{-1})	$1.88x10^{-10}$	$9.11x10^{-10}$
	j (J mol^{-1} K^{-2} Pa^{-2})	$3.11x10^{-16}$	$-5.92x10^{-15}$
	k (J mol^{-1} K^{-1} Pa^{-3})	$-1.10x10^{-20}$	$-2.15x10^{-20}$
	l (J mol^{-1} K^{-5})	$1.95x10^{-9}$	$2.48x10^{-9}$
	m (J mol^{-1} K^{-4} Pa^{-1})	$-1.59x10^{-8}$	$-7.50x10^{-8}$
	n (J mol^{-1} K^{-3} Pa^{-2})	$-1.59x10^{-13}$	$-7.50x10^{-13}$
	o (J mol^{-1} K^{-2} Pa^{-3})	$-9.09x10^{-19}$	$6.12x10^{-18}$

The compressibility factor and heat capacities at constant volume and pressure for the CO_2/CH_4 mixture were calculated using the surface equations and respective parameters present above and considering the Eqs. (A.1)-(A.3), valid for mixtures with a molar fraction up to 55 % of CO_2, temperatures from 180 to 480 K and pressures up to 80 bar:

$$Z = \sum_{i=1}^{n} y_i Z_i \tag{A.1}$$

$$C_p = \sum_{i=1}^{n} y_i C_{p,i} \tag{A.2}$$

$$C_v = \sum_{i=1}^{n} y_i C_{v,i} \tag{A.3}$$

Appendix AP - Complementary results

The profiles of the CO_2 molar fraction and the gas temperature for the adsorption step for case study 2 are presented in Figure AP.1:

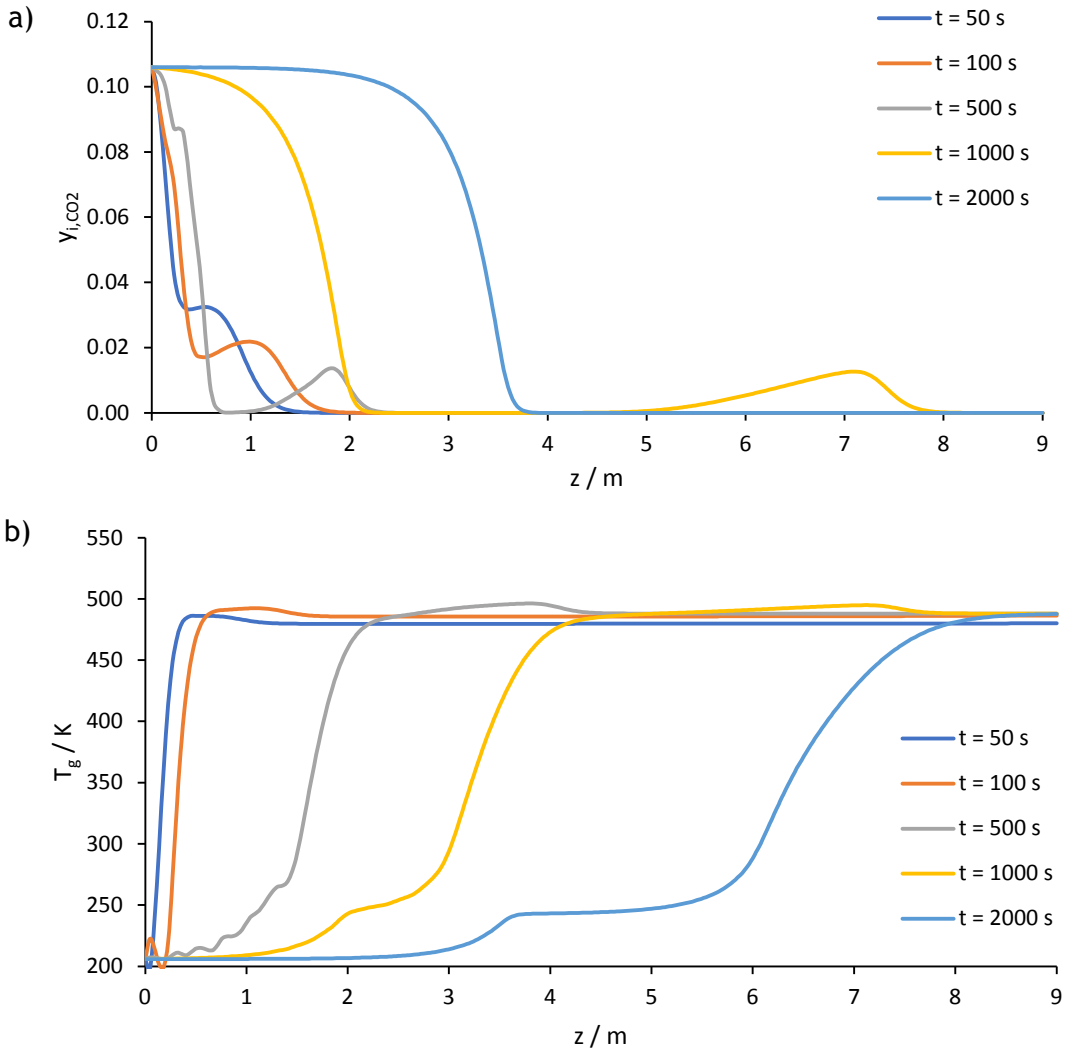

Figure AP.1 - Profiles for the adsorption step for case study 2: a) CO_2 molar fraction; b) gas temperature.